

International Journal of Modern Physics A  
 © World Scientific Publishing Company

## CONSTRUCTION OF LATTICE MÖBIUS DOMAIN WALL FERMIONS IN THE SCHRÖDINGER FUNCTIONAL SCHEME

YUKO MURAKAMI<sup>1,b</sup> and KEN-ICHI ISHIKAWA<sup>1,2,a</sup>

<sup>1</sup>*Graduate School of Science, Hiroshima University,  
 Higashi-Hiroshima, Hiroshima 739-8526, Japan*

<sup>2</sup>*Core of Research for the Energetic Universe, Hiroshima University,  
 Higashi-Hiroshima, Hiroshima 739-8526, Japan*

<sup>a</sup>*ishikawa@theo.phys.sci.hiroshima-u.ac.jp*

<sup>b</sup>*d152338@hiroshima-u.ac.jp*

In this paper, we construct the Möbius domain wall fermions (MDWFs) in the Schrödinger functional (SF) scheme for the SU(3) gauge theory by adding a boundary operator at the temporal boundary of the SF scheme setup. Using perturbation theory, we investigate the properties of several constructed MDWFs, including the optimal type domain wall, overlap, truncated domain wall, and truncated overlap fermions. We observe the universality of the spectrum of the effective four-dimensional operator at the tree-level, and fermionic contribution to the universal one-loop beta function is reproduced for MDWFs with a sufficiently large fifth-dimensional extent.

*Keywords:* Lattice Field Theory; Lattice Chiral Symmetry; Renormalization

PACS numbers:11.15.Ha,11.10.Gh,11.30.Rd

### 1. Introduction

Chiral symmetry has played an important role in quantum field theories and in the low-energy physics of Quantum Chromodynamics (QCD). Lattice field theory is a non-perturbative, first-principles framework for quantum field theories, and lattice gauge theory has been successfully applied to describing the low-energy properties of QCD.

Prior to mid-1990s, lattice QCD simulation faced major disadvantages in terms of a lack of chiral symmetry on the lattice arising from Nielsen-Ninomiya's no-go theorem, which implies the impossibility of constructing lattice fermions with chiral symmetry. Fortunately, the situation has changed following the development of theories for several lattice fermion, including: perfect action,<sup>1,2</sup> domain wall,<sup>3</sup> and overlap fermions.<sup>4-6</sup> The notion of symmetry in these lattice fermions can be summarized in terms of the Ginsparg-Wilson relation<sup>7</sup> and lattice chiral symmetry.<sup>8</sup> Overlap fermions exactly hold lattice chiral symmetry, while domain wall fermions hold an approximate symmetry with a finite extent in the fifth-dimension. Because lattice chiral symmetry is not chiral symmetry, the premise of the no-go theorem

is circumvented. Lattice chiral symmetry is associated with benefits found in continuum field theories such as no-fine tuning, no-operator mixing, *etc.*, and an early review on lattice chiral fermions can be found in Refs. 9-11.

Although lattice chiral fermion simulation cost is high, large-scale simulations of lattice QCD employing lattice chiral fermions, which can be supported by increasing computer performance, have been carried out in recent years.<sup>12</sup> It is necessary to renormalize the lattice operators in a usual manner. Non-perturbative renormalization schemes are preferable for reducing systematic errors in applications to involving QCD and Standard model calculations; hence, non-perturbative renormalization of lattice chiral fermions schemes have been sought.

Several non-perturbative renormalization schemes applicable to lattice field theories have been developed, including RI-MOM,<sup>13,14</sup> Schrödinger functional<sup>15-18</sup> (SF), and Gradient-flow.<sup>19-24</sup> The SF scheme has been successfully applied for Wilson type fermions to renormalize lattice operators, coupling, and fermion masses, together with the  $O(a)$ -improvements.<sup>15-18,25-35</sup> The application of the SF scheme to lattice chiral fermions represents a logical next step for extracting their renormalization factors non-perturbatively. The SF scheme employs a finite space-time box with a periodic boundary condition in the spatial directions and a Dirichlet boundary condition in the temporal direction; however the temporal boundary condition contradicts necessary conditions for overlap and domain wall fermions,<sup>36,37</sup> and it has been explicitly noted that the temporal boundary condition must violate chiral symmetry and the Dirac fermion propagator has a nontrivial anti-commutation relation to  $\gamma_5$  at the boundary in the continuum theory.<sup>38</sup> Therefore to reproduce the same property as in the continuum theory it is necessary to introduce an appropriate modification reflecting the boundary condition to the lattice chiral fermions. This means that the lattice chiral symmetry becomes nontrivial in the SF boundary condition.<sup>36-38</sup>

The SF scheme setup for lattice chiral fermions is formulated in Refs. 36-41. Lüscher investigated chiral symmetry with regard to the SF boundary condition in the continuum theory and pointed out a condition based on universality arguments under which the lattice chiral fermions could acquire a proper continuum limit, where the overlap fermion operator was modified through an explicit violation of the lattice chiral symmetry at the SF boundary.<sup>38</sup> The universality of the overlap fermion with the SF boundary condition was subsequently investigated perturbatively by Takeda,<sup>39</sup> who, in accordance with the universality argument in Ref. 38, introduced a boundary term for the domain wall fermion to formulate the SF scheme and investigated the property perturbatively.<sup>40</sup>

In this paper, we extend the work done by Takeda<sup>40</sup> to the Möbius domain wall fermions (MDWFs).<sup>42,43</sup> The MDWF is a generalization of the domain wall fermion involving the truncated overlap fermion, optimal domain wall fermion, and overlap fermion as limiting cases. One motivation for employing the MDWF is to reduce simulation cost through the use of a better approximate lattice chiral symmetry. After tuning the parameters contained in its action, the MDWF requires a smaller

extent in the fifth dimension than the standard domain wall fermion (SDWF) with the same approximate lattice chiral symmetry. When the parameters contained in the MDWF action are chosen optimally, which corresponds to the optimal domain wall fermion, lattice chiral symmetry can be realized numerically. Thus, the MDWF enables the performance of simulations under a controlled approximate lattice chiral symmetry in a cost-effective manner.<sup>43,44</sup> By developing the SF scheme for the MDWF, a class of lattice chiral fermions applicable to the SF scheme can be covered.

To find the boundary operator for the MDWF, it is necessary to identify the boundary term that properly breaks the chiral symmetry at the temporal boundary in the SF scheme. The boundary operator should hold the discrete space-time symmetries  $C$ ,  $P$ ,  $T$ , and  $\Gamma_5$ -Hermiticity, but it must break the lattice chiral symmetry at the temporal boundary only. In constructing the boundary term, we observe that the parameters of the MDWF, which depend on the fifth-index, must have parity symmetry in the fifth dimension in order to hold discrete symmetry. In this paper, we investigate the validity of the MDWF with a boundary term constructed by observing the continuum limit of the effective four-dimensional operator at the tree-level and the one-loop beta function perturbatively. Preliminary results of this work have been reported in Refs. 45, 46.

The paper is organized as follows. In section 2, we briefly introduce the SF formalism and the boundary condition and give the property of the Dirac propagator under chiral symmetry with the SF boundary condition.<sup>38</sup> Before proceeding to the construction of the MDWF with the SF boundary, we clarify the property of the MDWF in the periodic boundary condition in section 3. The continuum limit of the effective four-dimensional operator<sup>47,48</sup> is also examined to identify the normalization and the residual mass<sup>49</sup> at the tree-level. Section 4 describes the construction of the MDWF operator with the temporal boundary term in the SF. In section 5, we numerically verify the continuum limit of the effective four-dimensional operator and the propagator of the MDWF with the SF boundary at the tree-level. In a preliminary work,<sup>45</sup> we did not subtract the residual mass at the tree-level, resulting in non-universal behavior at a small extra-dimensional size and discovered that the residual mass must be subtracted to approach the correct continuum limit even at the tree-level. We also investigate the tree-level  $O(a)$ -improvement with the PCAC relation. In section 6, we verify the fermionic portion of the universal one-loop beta function and, in section 7, we conclude the paper.

## 2. Schrödinger Functional Scheme and Chiral Symmetry

In the Schrödinger Functional (SF) scheme,<sup>15–18</sup> the temporal and spatial extents are finite with lengths  $T$  and  $L$ , respectively. To enforce consistency with the time evolution of the quantum system, the Dirichlet boundary condition is imposed in the temporal direction. The temporal coordinate  $x_4$  is in  $[0, T]$ , while the spatial coordinate is  $x_j \in [0, L]$ . As we focus on the properties of the fermionic fields, we do not explain the details of the gauge field properties in the SF scheme in this paper.

4 *Yuko Murakami and Ken-Ichi Ishikawa*

We begin with the description of the fermionic fields in the continuum theory. The fermion field  $\psi(x)$  in the SF scheme has the following boundary conditions:

$$P_+ \psi(x)|_{x_4=0} = 0, \quad P_- \psi(x)|_{x_4=T} = 0, \quad (1)$$

$$\bar{\psi}(x) P_-|_{x_4=0} = 0, \quad \bar{\psi}(x) P_+|_{x_4=T} = 0, \quad (2)$$

with  $P_{\pm} = (1 \pm \gamma_4)/2$ . We employ the generalized periodic boundary condition in the spatial direction,

$$\psi(x_0, \mathbf{x} + L\hat{j}) = e^{i\theta_j} \psi(x_0, \mathbf{x}), \quad (3)$$

where  $\hat{j}$  is a unit vector in the  $j$ -th direction and  $\theta_j (j = 1, 2, 3)$  is a real parameter.

Although the mass-less Dirac propagator with the temporal boundary conditions given in Eqs. (1) and (2) anti-commutes with the  $\gamma_5$  operator

$$D\gamma_5 + \gamma_5 D = 0, \quad (4)$$

the mass-less Dirac propagator  $S(x, y)$  does not anti-commute with  $\gamma_5$  as in (5):

$$\gamma_5 S(x, y) + S(x, y) \gamma_5 = \int_{z_4=0} dz S(x, z) \gamma_5 P_- S(z, y) + \int_{z_4=T} dz S(x, z) \gamma_5 P_+ S(z, y). \quad (5)$$

This relation implies that a naive chiral symmetry does not hold in the SF scheme.<sup>38</sup>

On the lattice, the same SF boundary condition cannot be imposed directly on the MDWF field, as the MDWF is defined on a five-dimensional lattice. One required condition for lattice fermion actions in the SF scheme is that the lattice Dirac propagator should satisfy Eq. (5) in the continuum limit. Several modifications to the lattice chiral fermion actions to reproduce the SF boundary condition are discussed in Refs. 36–38, 40.

### 3. Properties of Möbius domain wall fermions in periodic boundary condition

Before introducing the SF scheme for MDWFs, we briefly explain the MDWF properties without the SF boundary condition. For simplicity, the following discussion assumes that the temporal and spatial extents of the lattice box are infinite or finite with periodic boundary conditions.

The MDWF operator<sup>42,43</sup>  $D_{\text{MDWF}}$  is defined by

$$D_{\text{MDWF}} = \begin{pmatrix} D_1^{(+)} & D_1^{(-)} P_L & 0 & 0 & 0 & -m_f D_1^{(-)} P_R \\ D_2^{(-)} P_R & D_2^{(+)} & D_2^{(-)} P_L & 0 & 0 & 0 \\ 0 & D_3^{(-)} P_R & D_3^{(+)} & D_3^{(-)} P_L & 0 & 0 \\ 0 & 0 & D_4^{(-)} P_R & D_4^{(+)} & D_4^{(-)} P_L & 0 \\ 0 & 0 & 0 & D_5^{(-)} P_R & D_5^{(+)} & D_5^{(-)} P_L \\ -m_f D_6^{(-)} P_L & 0 & 0 & 0 & D_6^{(-)} P_R & D_6^{(+)} \end{pmatrix}, \quad (6)$$

$$D_j^{(+)} = D_W b_j + 1, \quad D_j^{(-)} = D_W c_j - 1, \quad (j = 1, 2, \dots, N_5), \quad (7)$$

where  $P_{L/R} = (1 \mp \gamma_5)/2$ ,  $D_W$  is the four-dimensional Wilson-Dirac operator with a negative mass ( $-m_0$ ), which corresponds to the domain wall height, and  $m_f$  is the fermion mass. The size in the fifth dimension  $N_5$  is assumed to be an even number, and we use  $N_5 = 6$  to explicitly display the operator in five-dimensional form throughout this paper. The coefficients  $b_j$  and  $c_j$  are tunable parameters of the MDWF chosen to optimize the lattice chiral symmetry with a minimum computational cost at a finite  $N_5$ . In this paper, we generally use  $a = 1$  as the lattice spacing “ $a$ ” while writing  $a$  explicitly when dealing with the continuum limit.

We employ the MDWF action  $S_q$  defined by

$$S_q = \bar{\Psi} D_{\text{MDWF}}^{(N_5)} \Psi + \frac{1}{2} \Phi^* D_{\text{PV}}^{(N_5)} \Phi, \quad (8)$$

where  $\Psi$  is the five-dimensional fermion field and  $\Phi$  the Pauli-Villars field.  $D_{\text{PV}}^{(N_5)}$  is defined by  $D_{\text{PV}}^{(N_5)} = D_{\text{MDWF}}^{(N_5)}|_{m_f=1}$  which eliminates all except the lightest massive mode from the spectrum. Integrating  $\Psi$  and  $\Phi$  out in the path-integral with this action, the fermionic determinant can be expressed<sup>47,48</sup> as

$$\det[D_{\text{MDWF}}^{(N_5)}/D_{\text{PV}}^{(N_5)}] = \det[D_{\text{eff}}^{(N_5)}], \quad (9)$$

where  $D_{\text{eff}}^{(N_5)}$  is the effective four-dimensional operator. The explicit form of the effective four-dimensional operator  $D_{\text{eff}}^{(N_5)}$  in terms of the MDWF operator (6) is given by

$$D_{\text{eff}}^{(N_5)} \equiv \epsilon^T P^T \left( D_{\text{PV}}^{(N_5)} \right)^{-1} D_{\text{MDWF}}^{(N_5)} P \epsilon. \quad (10)$$

The permutation and chiral projection matrix  $P$  and the restriction vector  $\epsilon$  are defined by

$$P = \begin{pmatrix} P_L & P_R & 0 & 0 & 0 & 0 \\ 0 & P_L & P_R & 0 & 0 & 0 \\ 0 & 0 & P_L & P_R & 0 & 0 \\ 0 & 0 & 0 & P_L & P_R & 0 \\ 0 & 0 & 0 & 0 & P_L & P_R \\ P_R & 0 & 0 & 0 & 0 & P_L \end{pmatrix}, \quad \epsilon = (1, 0, 0, 0, 0, 0)^T. \quad (11)$$

In the periodic or infinite volume case, we can obtain the explicit form for the four-dimensional operator as<sup>42,43,50–53</sup>

$$D_{\text{eff}}^{(N_5)} = \frac{1 + m_f}{2} + \frac{1 - m_f}{2} \gamma_5 R_{N_5}(\mathcal{H}_W). \quad (12)$$

The matrix function  $R_{N_5}(x)$  in Eq. (12) is the rational approximation to the signum function

$$R_{N_5}(x) = \frac{\prod_{j=1}^{N_5} (1 + w_j x) - \prod_{j=1}^{N_5} (1 - w_j x)}{\prod_{j=1}^{N_5} (1 + w_j x) + \prod_{j=1}^{N_5} (1 - w_j x)}. \quad (13)$$

6 *Yuko Murakami and Ken-Ichi Ishikawa*

The matrix  $\mathcal{H}_W$  in the argument is given by

$$\mathcal{H}_W = \gamma_5 D_W (a_5 D_W + 2)^{-1}. \quad (14)$$

The coefficients  $(w_j, a_5)$  have the following relation to the MDWF parameters  $(b_j, c_j)$ :

$$b_j + c_j = w_j, \quad b_j - c_j = a_5. \quad (15)$$

This is one of the parameter choice, as the normalization of  $\mathcal{H}_W$  can be absorbed into the definition of  $w_j$ . To be specific, we employ the following parametrizations for the Shamir and overlap kernels:

$$\mathcal{H}_W = \gamma_5 D_W (D_W + 2)^{-1}, \quad \text{with } b_j + c_j = w_j, b_j - c_j = 1, \quad (16)$$

for the Shamir kernel and

$$\mathcal{H}_W = \gamma_5 D_W, \quad \text{with } b_j = c_j = w_j, \quad (17)$$

for the overlap kernel. We investigate these two kernels throughout the paper.

The effective four-dimensional operator in Eq. (12) reduces to the overlap operator in the limit  $N_5 \rightarrow \infty$  provided by the convergence of the approximation to the signum function with a given  $(b_j, c_j)$ . We can define an effective four-dimensional fermion theory with Eq. (10) at a finite  $N_5$  with the following action;

$$S_{q\text{eff}} = \bar{\psi} D_{\text{eff}}^{(N_5)} \psi, \quad (18)$$

where  $\psi$  is the fermion field on the four-dimensional lattice. We call this theory as the truncated overlap fermion because  $R_{N_5}(x)$  in Eq. (13) is a truncation of the signum function approximation and Eq. (12) is an approximation to the overlap fermion operator at a finite  $N_5$ .

The MDWF operator generalizes the domain wall type fermion operators, which include the standard domain wall, Boriçi's domain wall,<sup>50-52</sup> and optimal Chiu's domain wall<sup>53</sup> fermions. The overlap operator,  $D_{\text{OVF}}$ , in the limiting case satisfies the Ginsparg-Wilson (GW) relation<sup>7</sup>

$$\gamma_5 D_{\text{OVF}} + D_{\text{OVF}} \gamma_5 = \frac{2}{1 + m_f} (m_f \gamma_5 + D_{\text{OVF}} \gamma_5 D_{\text{OVF}}). \quad (19)$$

At a finite  $N_5$ , the effective four-dimensional operator  $D_{\text{eff}}^{(N_5)}$  does not satisfy the GW relation owing to the explicit breaking of the lattice chiral symmetry. To investigate the chiral property in the SF scheme at a finite  $N_5$ , this explicit breaking must be taken into account. Taking the continuum limit of Eq. (12) at the tree-level,

we obtain

$$aD_{\text{eff}}^{(N_5)} \rightarrow Z [ia\cancel{\partial} + am_{\text{res}}], \quad (20)$$

$$Z = \frac{(1 - am_f)R_{N_5}(\alpha)}{(am_0)(2 - (am_0)a_5)}, \quad (21)$$

$$am_{\text{res}} = \left[ \frac{1 + am_f}{1 - am_f} \frac{1}{R_{N_5}(\alpha)} - 1 \right] \frac{(am_0)(2 - (am_0)a_5)}{2}, \quad (22)$$

$$\alpha = \frac{(am_0)}{2 - (am_0)a_5}. \quad (23)$$

There is a residual mass  $am_{\text{res}}$  in  $D_{\text{eff}}^{(N_5)}$  even at the tree-level with  $m_f = 0$ .<sup>49</sup> However, the residual mass vanishes in  $N_5 \rightarrow \infty$  as  $R_{N_5}(\alpha) \rightarrow 1$ .

The analysis in this section is based on the explicit form of the effective four-dimensional operator in Eq. (12). In the next section we introduce an MDWF operator for the SF scheme by modifying Eq. (6). Although the normalization  $Z$  of Eq. (21) and the residual mass  $am_{\text{res}}$  of Eq. (22) are obtained in the periodic boundary condition, we use these to renormalize the modified MDWF operator with the SF boundary condition at the tree-level.

#### 4. Möbius domain wall fermions with the Schrödinger functional boundary condition

The SF scheme is defined in a finite four-dimensional box in which the lattice extents in the spatial and temporal directions are  $N_S = L/a$  and  $N_T = T/a$ , respectively. The lattice index in the spatial direction  $n_k, k = 1, 2, 3$  covers  $0, 1, \dots, N_S - 1$ , while the temporal index  $n_4$  covers  $1, 2, \dots, N_T - 1$ . The fields at  $n_4 = 0$  and  $n_4 = N_T$  are fixed using the Dirichlet boundary conditions (1) and (2).

According to the universality argument given by Lüscher<sup>38</sup> and the realization of the SF scheme for the standard domain wall fermion by Takeda,<sup>40</sup> we modify the MDWF operator in Eq. (6) by adding a boundary operator  $B_{\text{SF}}$  as follows:

$$D_{\text{MDWF}}^{\text{SF}} = D_{\text{MDWF}} + c_{\text{SF}} B_{\text{SF}}, \quad (24)$$

$$B_{\text{SF}} = \begin{pmatrix} 0 & 0 & 0 & 0 & 0 & -D_1^{(-)}B \\ 0 & 0 & 0 & 0 & -D_2^{(-)}B & 0 \\ 0 & 0 & 0 & -D_3^{(-)}B & 0 & 0 \\ 0 & 0 & D_3^{(-)}B & 0 & 0 & 0 \\ 0 & D_2^{(-)}B & 0 & 0 & 0 & 0 \\ D_1^{(-)}B & 0 & 0 & 0 & 0 & 0 \end{pmatrix}. \quad (25)$$

The boundary operator  $B$  is defined by

$$B(n, m) = \delta_{n,m} \gamma_5 (\delta_{n_4,1} P_- + \delta_{n_4, N_T - 1} P_+). \quad (26)$$

The temporal hopping terms from  $n_4 = 0$  and  $n_4 = N_T$  in the Wilson-Dirac operator contained in Eq. (24) are set to zero as the SF boundary condition. The operators

in the action Eq. (8) are replaced with Eq. (24) in the SF scheme. Hereafter we omit the superscript SF on the operator in the SF scheme to simplify the notation.

$B_{\text{SF}}$  has supports only at  $n_4 = 1$  and  $N_T - 1$ , and explicitly violates the domain wall chiral symmetry<sup>54</sup> at these points; we expect, however, that the lattice chiral symmetry is still maintained in the bulk region. The coefficient  $c_{\text{SF}}$  is a nonzero parameter for removing the  $O(a)$ -discretization error from the boundary effect. Although the form of  $B_{\text{SF}}$  is a naive extension of Takeda's realization, we require its parity symmetry in the fifth-direction to maintain the discrete symmetries,  $C, P, T$  and  $\Gamma_5$ -Hermiticity. Although this parity symmetry is not required in the periodic boundary or infinite extent cases, it seems to be of theoretical benefit in the analysis of the corresponding operator and action.<sup>42,54-57</sup>

The effective four-dimensional operator for Eq. (24) is defined by Eq. (10); however, we could not extract a simple short form for the effective four-dimensional operator similar to Eq. (12). As seen from Eq. (12), the ordering of  $b_j$  and  $c_j$  are irrelevant in the periodic or infinite volume cases but affect the form of the effective four-dimensional operator in the SF scheme, *i.e.*, a different choice for the ordering yields a different effective operator. This ordering dependence must disappear in the continuum limit, as the SF scheme is regularization independent.

At a finite  $N_5$ , the degree of freedom required for  $b_j$  and  $c_j$  to optimize the lattice chiral symmetry with the SF boundary is halved from that without the SF boundary as a result of the parity symmetry constraint. Therefore, we cannot use the optimal choices for  $b_j$  and  $c_j$  as given, *e.g.*, by Chiu.<sup>53</sup> Choices for the coefficients are given in Refs. 55, 56 and optimal coefficients with the parity constraint are formulated in Ref. 58. Instead of the optimal coefficients, however, we employ quasi-optimal coefficients in which the half-order ( $N_5/2$ ) coefficients from the Zolotarev optimal coefficients<sup>53,59</sup> are duplicated to construct the  $N_5$  coefficients. The property of quasi-optimal choice was surveyed in our previous study,<sup>45</sup> in which we checked that the discrepancies between quasi-optimal and optimal coefficients<sup>58</sup> were small for  $N_5 \gtrsim 10$ .

Although we cannot extract the rational approximation  $R_{N_5}(x)$  with the boundary term  $B_{\text{SF}}$ , we assume that the same rational form is valid in the bulk region because the boundary effect becomes small as the temporal extent is increased. For the same reason, we use this form for the normalization  $Z$  and the residual mass  $am_{\text{res}}$  for the SF boundary. The choice of coefficients  $b_j$  and  $c_j$  is still important to maintain the lattice chiral symmetry in the bulk region; to determine the corresponding values of the coefficients from the approximation range for the signum function, we use the spectrum of the kernel operator in Eq. (14) with the Wilson-Dirac fermion operator  $D_W$  satisfying the SF boundary condition.

## 5. Tree-Level Analysis of Möbius Domain Wall Fermions with the SF boundary condition

In this section, we investigate the properties of the effective four-dimensional operator built with the MDWF with the SF boundary term in Eq. (24) at the tree-level. The spectrum, temporal structure of the GW relation, and propagator are all investigated at the tree-level. After checking the universality to the continuum limit, we will examine the fermionic contribution to the one-loop beta function in the next section. In this paper, we employ the Euclidean form<sup>60</sup> of the Dirac representation<sup>61</sup> for the Dirac gamma matrices.

The classical background field induced by the SF boundary gauge field must be incorporated in the analysis with respect to the one-loop beta function. The classical background gauge field<sup>17</sup> is given by

$$U_k(n) = \exp \left[ i \frac{1}{N_T} (n_4 \phi'_k + (N_T - n_4) \phi_k) \right], \quad U_4(n) = 1. \quad (27)$$

This is induced by the boundary field

$$U_k(n)|_{n_4=0} = e^{i\phi_k}, \quad U_k(n)|_{n_4=N_T} = e^{i\phi'_k}, \quad (28)$$

for the spatial gauge fields ( $k = 1, 2, 3$ ) at  $n_4 = 0$  and  $N_T$ .<sup>17</sup> The standard choices for  $\phi_k$  and  $\phi'_k$  defining the SF coupling<sup>17</sup> are

$$\begin{aligned} \phi_k &= \frac{1}{N_S} \text{diag} \left( \eta\omega_1 - \frac{\pi}{3}, \eta\omega_2, \eta\omega_3 + \frac{\pi}{3} \right), \\ \phi'_k &= \frac{1}{N_S} \text{diag} \left( -\eta\omega_1 - \pi, -\eta\omega_3 + \frac{\pi}{3}, -\eta\omega_2 + \frac{2\pi}{3} \right), \\ (\omega_1, \omega_2, \omega_3) &= (1, -1/2, -1/2). \end{aligned} \quad (29)$$

This set of choices induces a nonzero chromo-electric field as the background field. Another choice for the boundary condition is  $\phi_k = 0$  and  $\phi'_k = 0$ , which is useful for analyzing the Dirac propagator analytically in the continuum theory.

The effective four-dimensional operator is renormalized using Eqs. (21) and (22) as

$$D_q = Z^{-1} D_{\text{eff}}^{(N_5)}. \quad (30)$$

In the following, we will investigate the spectrum, the chiral property in the GW relation, and the propagator of the renormalized  $D_q$  with and without the background field.

### 5.1. Spectrum of the effective four-dimensional operator

In this section, we investigate the spectrum of the Hermitian squared effective four-dimensional operator  $D_q^\dagger D_q$  in boxes with  $N_T = N_S$  with and without the nonzero background field. We show that the cases  $b_j = c_j = w_j$  correspond to the overlap fermion in the  $N_5 \rightarrow \infty$  limit. This choice is a nontrivial check to the standard domain wall fermion because  $c_j \neq 0$  is the new structure for the MDWF.

Table 1. MDWF parameters  $b_j (= c_j)$  corresponding to signum function approximation parameters  $w_j = b_j$ .

$j$	$b_j$
1, 8	0.237921110807
2, 7	1.265028710883
3, 6	11.29279846601
4, 5	60.04391219119

The quasi-optimal values for the MDWF parameters  $(b_j, c_j)$  are determined by specifying the approximation range and the order  $N_5/2$  of the Zolotarev approximation formula. We use the spectrum of the kernel operator in Eq. (14) to determine the approximation range. We investigate the lowest and highest eigenvalues of the kernel operator with the SF background field and  $\theta = \pi/5$ ,<sup>62</sup> obtaining

$$0.361893 \frac{1}{N_S} < a|\mathcal{H}_W| < 1.0, \quad (31)$$

for the Shamir kernel in Eq. (16) and

$$0.725254 \frac{1}{N_S} < a|\mathcal{H}_W| < 7.0, \quad (32)$$

for the overlap kernel in Eq. (17) from the asymptotic behavior to the continuum limit. The lowest eigenvalue approaches zero as we take the continuum limit by fixing  $L = aN_S$  as a constant; this means that the approximation to the signum function becomes worse with a fixed  $(b_j, c_j)$  when the lower spectrum spills over the approximation range in taking the continuum limit.

The MDWF parameters  $b_j$  and  $c_j$  used in the spectrum test, as obtained from the  $N_5 = 4$  optimal Zolotarev approximation coefficient, are listed in Table 1. The signum function approximation range and the accuracy of the original coefficients  $w_j (j = 1, \dots, 4)$  are  $x \in [0.01, 7.00]$  and  $|1 - R_4(x)| \lesssim 0.324$ , respectively. As seen from Eq. (32), this approximation is valid with  $N_S < 72$  in the cases with the SF background field and  $\theta = \pi/5$ . The signum function with the parity-symmetric coefficients in the fifth dimension,  $w_j (j = 1, \dots, 8)$ , has an accuracy of  $|1 - R_8(x)| \lesssim 0.072$  (Fig. 1).

The lowest ten eigenvalues at  $am_{\text{res}} = 0$  are shown in Figure 2 as a function of  $a/L = 1/N_S$ . The boundary coefficient is  $c_{\text{SF}} = 1$ . The solid circles at  $a/L = 0$  are the eigenvalues in continuum theory.<sup>16,62</sup> We use  $Z = 0.99659683271$  to normalize Eq. (21) and  $am_{\text{cr}} = -0.0034031673$ , where  $am_{\text{res}}|_{am_f=am_{\text{cr}}} = 0$  from Eq. (22).

The spectrum properly converges to the continuum limit even at a smaller  $N_5 = 8$ , which supports the use of the normalization in Eq. (21) and residual mass subtraction in Eq. (22) even with the SF boundary condition. We confirm

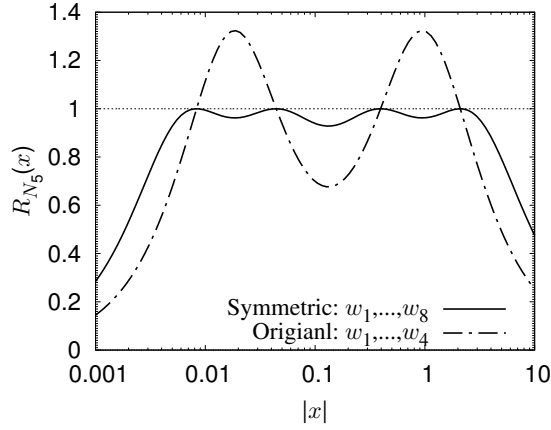
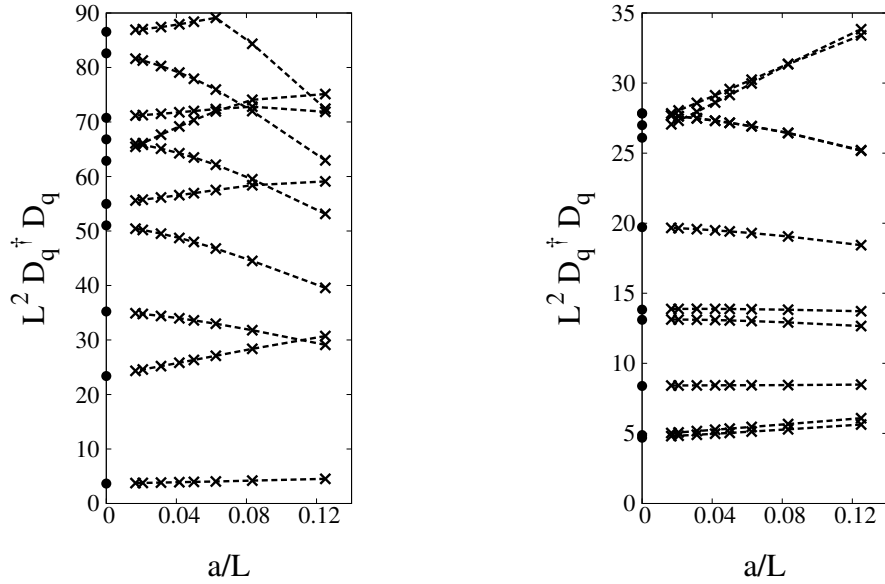


Fig. 1. Signum function approximation based on Eq. (13). “Original” uses  $w_1, \dots, w_4$ , which corresponds to the fourth-order optimal Zolotarev approximation, while “Symmetric” uses all coefficients from Table 1.



(a) Without the background field ( $\phi_k = \phi'_k = 0$ ).

(b) With the background field ( $\phi_k|_{\eta=0}, \phi'_k|_{\eta=0}$ ).

Fig. 2. Ten lowest eigenvalues of the MDWF with  $c_j = b_j = w_j$ ,  $N_5 = 8$ ,  $am_{\text{res}} = 0$ ,  $\theta = \pi/5$  and  $c_{\text{SF}} = 1$ . The  $w_j$  are taken from the optimal Zolotarev approximation with the approximation range  $x \in [0.01; 7.00]$  at the given order.

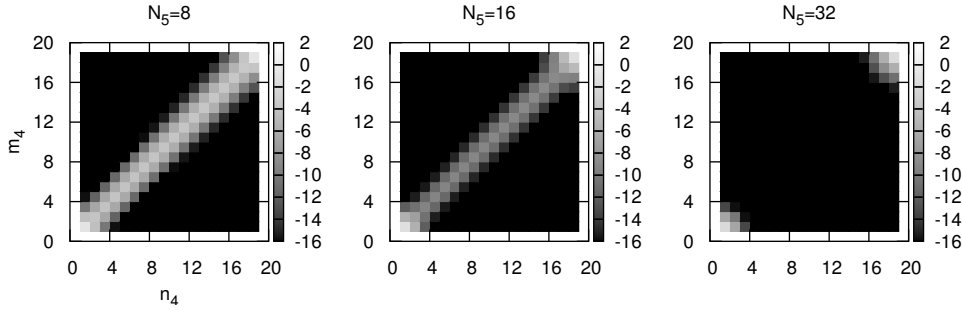
12 *Yuko Murakami and Ken-Ichi Ishikawa*

Fig. 3. GW relation violation (33) of the MDWF with  $c_j = b_j = w_j$  and  $c_{\text{SF}} = 1$ . The  $w_j$  are taken from the optimal Zolotarev approximation with the approximation range  $x \in [0.01, 7.00]$  at the given order. The data are evaluated on the background fields (28) with (29) with  $\eta = 0$ .

the same behavior for other parameters, namely, larger values of  $N_5$ ,  $am_{\text{res}} \neq 0$ , a reverse order of  $b_j$ , and other overlap kernels ( $b_j + c_j = 1$ ) and ( $b_j = 1, c_j = 1$ ).

## 5.2. Dirac propagator from the effective four-dimensional operator

In this section, the GW relation for the effective operator  $D_q(n, m)$  and the properties of the propagator  $S(n, m) \equiv (D_q)^{-1}(n, m)$  in the temporal direction are investigated at vanishing spatial momentum and mass. The GW relation violation is measured using

$$\delta(n_4, m_4) = \sum_{\text{color, spin}} \left| \{\gamma_5, \tilde{D}_q(n_4, m_4)\} - 2\tilde{D}_q(n_4, m_4)\gamma_5\tilde{D}_q(n_4, m_4) \right|, \quad (33)$$

where  $\tilde{D}_q(n_4, m_4)$  is the zero-momentum portion of  $D_q(n, m)$ .

Figure 3 shows the GW relation violation with the background field,  $\theta = \pi/5$  and the boundary coefficient  $c_{\text{SF}} = 1$ . We employ the operator  $c_j = b_j = w_j$  applying the quasi-optimal approximation, and the approximation range is fixed to  $x \in [0.01, 7.00]$  for all  $N_5$ . The gray scale corresponds to  $\log_{10}(\delta(n_4, m_4))$ . As  $N_5$  increases, the violation in the bulk temporal region vanishes but remains at the temporal boundary as expected. The same behavior is observed for other kernel operators with different parameters.

The Dirac propagator with the SF boundary condition has been analytically obtained in the continuum theory.<sup>16,63</sup> Figs 4 and 5 show the time dependence of the real part of the spin (1,1)-component of the Dirac propagator using the Dirac representation for the  $\gamma$ -matrices. The boundary coefficient is  $c_{\text{SF}} = 1$  and the source times are  $m_4 = 1$  and 2 in Figs. 4 and 5, respectively. The solid line represents the analytic solution in the continuum theory. The cut-off dependence of the lattice propagator can be compared at  $L/a = N_S = 10$  (crosses) and  $L/a = N_S = 40$  (open circles).

From the left panel (4(a)), we see that the propagator with the standard domain wall fermion ( $b_j = 1, c_j = 0$ ) converges to the continuum limit properly. On the

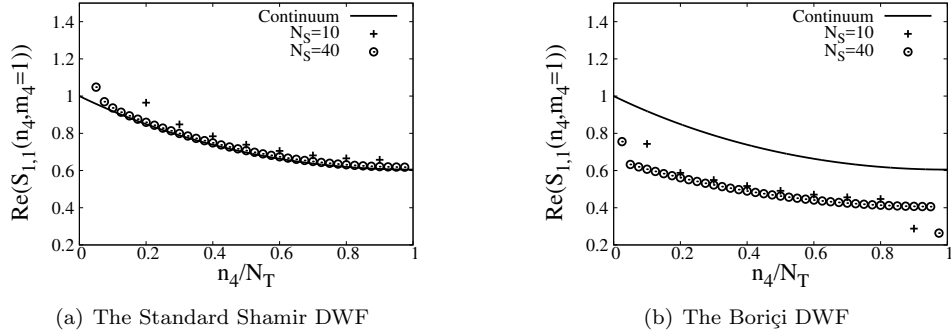


Fig. 4. Real part of the spin (1,1)-component of the Dirac propagator from  $m_4 = 1$ . The data are evaluated at  $am_{res} = 0$ ,  $am_0 = 1.0$ ,  $\theta = \pi/5$ , and  $N_5 = 16$  on the zero background field ( $\phi_k = 0$  and  $\phi'_k = 0$ ).

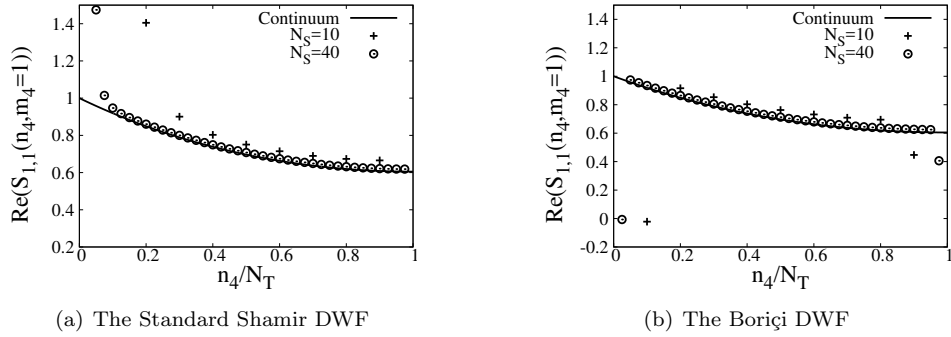


Fig. 5. Real part of the spin (1,1)-component of the Dirac propagator from  $m_4 = 2$ .

other hand, in the right panel (4(b)) the propagator with the Boriçi domain wall fermion ( $b_j = 1, c_j = 1$ )<sup>50–52</sup> does not converge to the continuum line. To check the boundary effect further, we plot the Dirac propagator propagating from  $m_4 = 2$  in Figure 5. The left panel (5(a)) shows the standard domain wall fermion and is consistent with the continuum limit. The Boriçi domain wall fermion in the right panel (5(b)) is now consistent with the continuum limit. Although the boundary coefficient  $c_{SF}$  can be tuned to eliminate the boundary  $O(a)$  error, it is seen from Figure 4(b) that the discrepancy is not proportional to  $a$  and cannot be removed by tuning  $c_{SF}$ . We have shown the propagator in the vanishing background field so far, the same behavior is seen on the non-zero background field defined by Eqs. (27)–(29) with  $\eta = 0$ , in which the color degeneracy is resolved.

To better understand the property of the discrepancy, we investigated the ratio of the propagator of the Boriçi domain wall fermion to that under continuum theory and take the continuum limit. We employ  $c_{SF} = 0.4167$ , which is determined by the

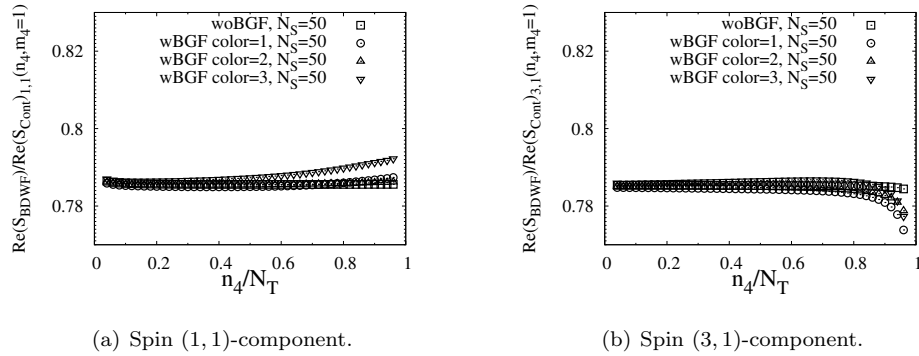


Fig. 6. The ratio of the real part of the Boriçi DWF propagator to the continuum theory. The source time is  $m_4 = 1$ . Squares are for the vanishing background field, while circles, up-, and down-triangles are for the non-zero background field defined by Eqs. (27)–(29) with  $\eta = 0$ . The data are evaluated with  $c_{SF} = 0.4167$ ,  $am_{res} = 0$ ,  $am_0 = 1.0$ ,  $\theta = \pi/5$ , and  $N_5 = 16$ .

PCAC relation to be described in the next subsection, to eliminate the dominant  $O(a)$  error in taking the continuum limit. We also investigate the dependence of the discrepancy on the presence of the background field. Figure 6 shows the time dependence of the ratio of the lattice Dirac propagator to the continuum Dirac propagator. We observe that the discrepancy is almost constant in time and slightly depends on the color index. Figure 7 shows the continuum extrapolation for the ratios at the sink time slices at  $n_4 = N_T/4, N_T/2$ , and  $3N_T/4$ . As we employ  $c_{SF} = 0.4167$  for the boundary  $O(a)$ -improvement, the dominant cut-off dependence is of  $O(a^2)$ . The dotted lines in the figure show the fitting results with  $c + d/N_T^2$  on the data in  $< 1/N_T = 1/80$  without any constraints on the fitting parameters. The discrepancy converges to a common value (this case  $\simeq 0.7856(6)$ ) irrespective of the spin components, sink time, and the presence of the background field in the continuum limit. We also obtain the same constant value for the other source time  $m_4 = N_T - 1$ . Figure 8 shows the propagator from the source time at  $m_4 = N_T/20$ , which is close to the boundary, but the physical distance from the boundary is kept fixed at  $am_4 = y_4 = T/20$ . As seen in Figure 8(a), the propagator with  $N_S = 20$  (up-triangles) shows a large deviation from the continuum theory as  $m_4 = 20/20 = 1$ , while that with  $N_S = 40$  (circles) almost overlaps on the continuum theory. The propagator properly converges to the continuum theory as in Figure 8(b).

We found that this phenomenon, a constant factor discrepancy in the continuum limit remains in the propagator at the surface time slices  $n_4 = 1$  and  $n_4 = N_T - 1$  (the interior time surfaces of the SF boundary condition) is common to other MDWFs with  $c_j \neq 0$  we investigated. This strongly suggests the presence of the boundary effect introduced by Eq. (25). As we put the boundary term  $B_{SF}$  at  $n_4 = 1$  and  $N_T - 1$  in the MDWF operator, contact terms with  $B_{SF}$  and the fermion field operators of the effective four-dimensional theory could exist at the surface time

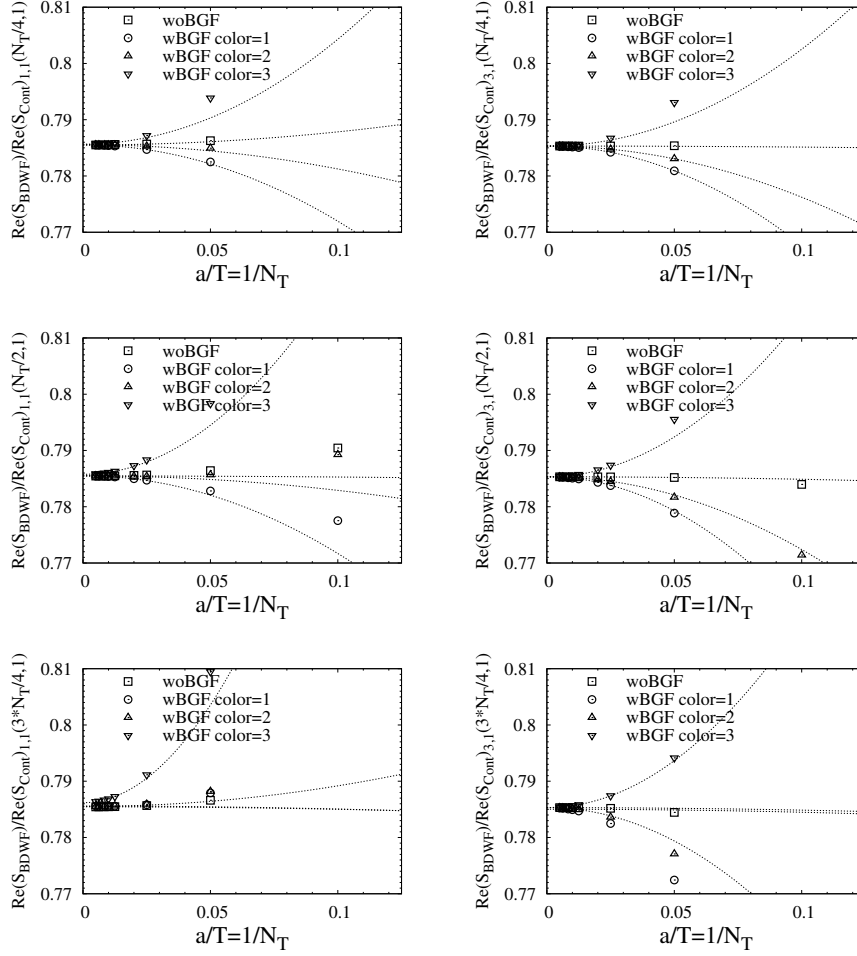
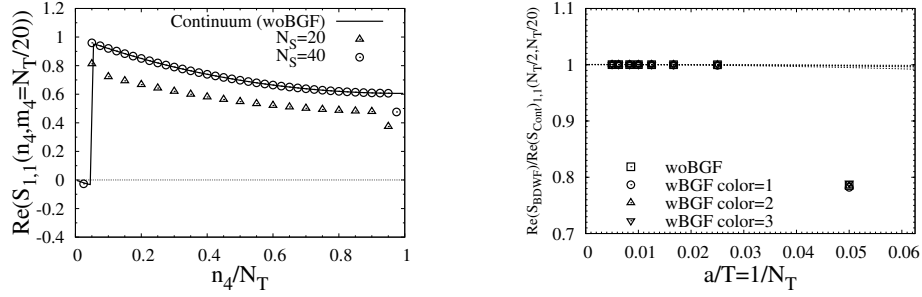


Fig. 7. Continuum limit extrapolation for the ratios of the Boriçi DWF propagator to the continuum theory (from top to bottom : time slices at  $n_4 = N_T/4, N_T/2$  and  $3N_T/4$ , left column : spin  $(1, 1)$ -component, right column : spin  $(3, 1)$ -component). The data are evaluated with  $c_{SF} = 0.4167$ ,  $am_{res} = 0$ ,  $am_0 = 1.0$ ,  $\theta = \pi/5$ , and  $N_5 = 16$ .

slices.

From these observations, we can conclude that a constant renormalization is needed for the propagator touching the surface time slices. This phenomenon has been also observed in the overlap fermion in the SF scheme.<sup>38</sup> A degree of freedom is available to renormalize the boundary operators or fields of the fermion fields.<sup>16, 18, 63, 64</sup> The boundary fields at  $n_4 = 0$  and  $n_4 = N_T$  in the SF scheme can be renormalized independently from the bulk fermion fields and the renormalization for the boundary fields has been introduced for the overlap fermion in Ref. 38. We briefly show the definition of the boundary fields in the SF scheme<sup>16, 18, 38, 64</sup> in

16 *Yuko Murakami and Ken-Ichi Ishikawa*


(a) Real part of spin (1,1)-component of the Dirac propagator in the vanishing background field.

(b) Continuum limit extrapolation at the sink time  $n_4 = N_T/2$ .

Fig. 8. Tho Boriçi DWF propagator from the source time  $m_4 = N_T/20$ . The data are evaluated using the Boriçi DWF with  $c_{SF} = 0.4167$ ,  $am_{res} = 0$ ,  $am_0 = 1.0$ ,  $\theta = \pi/5$ , and  $N_5 = 16$ .

the following. After introducing the definition, we discuss two possibilities for the renormalization on the surface time slices using the boundary fields.

In the SF scheme, instead of the Dirichlet boundary condition (Eqs. (1) and (2)), the following inhomogeneous boundary condition,

$$P_+ \psi(x)|_{x_4=0} = \rho(\mathbf{x}), \quad P_- \psi(x)|_{x_4=T} = \rho'(\mathbf{x}), \quad (34)$$

$$\bar{\psi}(x)P_-|_{x_4=0} = \bar{\rho}(\mathbf{x}), \quad \bar{\psi}(x)P_+|_{x_4=T} = \bar{\rho}'(\mathbf{x}), \quad (35)$$

can be imposed on the fermion field in the continuum theory. The three-dimensional fields,  $\rho(\mathbf{x})$  and  $\rho'(\mathbf{x})$ , act as the auxiliary source fields and considered as functional parameters of the partition function in the SF scheme.<sup>16, 18, 64</sup> The inhomogeneous boundary condition can not be imposed directly on the lattice fields in the bulk temporal region and it emerges after taking the continuum limit of the lattice theory provided that the lattice action contains proper couplings to the boundary fields  $\rho, \rho', \bar{\rho}, \bar{\rho}'$ . According to the method described in Ref. 38, instead of adopting the inhomogeneous boundary condition (Eqs. (34) and (35)), we employ the homogeneous boundary condition (Eqs. (1) and (2)) and introduce the boundary quark fields directly by

$$\begin{aligned} \zeta(\mathbf{x}) &= P_- \psi(x)|_{x_4=0}, & \zeta'(\mathbf{x}) &= P_+ \psi(x)|_{x_4=T} \\ \bar{\zeta}(\mathbf{x}) &= \bar{\psi}(x)P_+|_{x_4=0}, & \bar{\zeta}'(\mathbf{x}) &= \bar{\psi}(x)P_-|_{x_4=T} \end{aligned} \quad (36)$$

in the continuum theory.

A possible form for the boundary fermion fields on the lattice<sup>38, 40</sup> is

$$\begin{aligned} \zeta(\mathbf{n}) &= U_4(n - \hat{4})P_- \psi(n)|_{n_4=1}, & \zeta'(\mathbf{n}) &= U_4(n)^\dagger P_+ \psi(n)|_{n_4=N_T-1} \\ \bar{\zeta}(\mathbf{n}) &= \bar{\psi}(n)P_+ U_4(n - \hat{4})^\dagger|_{n_4=1}, & \bar{\zeta}'(\mathbf{n}) &= \bar{\psi}(n)P_- U_4(n)|_{n_4=N_T-1}, \end{aligned} \quad (37)$$

where  $\psi(n)$  is the effective four-dimensional fermion field in the bulk temporal region and  $\hat{4}$  is a lattice unit vector in the temporal direction.

Including these boundary fields together with the fermion fields in the bulk time slices, various fermionic correlation functions (Wick contractions) are introduced to probe the system;  $\overline{\zeta'(\mathbf{n})\psi(m)}$ ,  $\overline{\zeta'(\mathbf{n})\zeta(\mathbf{m})}$ ,  $\overline{\psi(n)\psi(m)}$ , ... *etc.* For the PCAC relation, which will be described in the next subsection, the correlation function  $\overline{\psi(n)\zeta(\mathbf{m})}$  is used and Eq. (37) leads to

$$\overline{\psi(n)\zeta(\mathbf{m})} = S(n, m)P_+U_4^\dagger(m - \hat{4})\Big|_{m_4=1}. \quad (38)$$

Now we discuss two possibilities for the renormalization on the surface time slices using the boundary fields. The boundary-bulk propagator, Eq. (38), shows that the discrepancy in  $S(n, m)|_{m_4=1}$  can be absorbed into the redefinition of the boundary fields through

$$\zeta_R(\mathbf{n}) = Z_\zeta\zeta(\mathbf{n}), \quad \zeta'_R(\mathbf{n}) = Z_\zeta\zeta'(\mathbf{n}), \quad \bar{\zeta}_R(\mathbf{n}) = Z_\zeta\bar{\zeta}(\mathbf{n}), \quad \bar{\zeta}'_R(\mathbf{n}) = Z_\zeta\bar{\zeta}'(\mathbf{n}), \quad (39)$$

with a constant  $Z_\zeta$ .<sup>18,63,64</sup> This normalization method has been adopted in Ref. 38 for the overlap fermion to recover the canonical normalization for the propagators that involve the boundary fields. One required condition for the renormalization via the boundary fields is the localization of the discrepancy at the boundaries. and the localization requires that the discrepancy should not depend on the global property of the system. As seen in Figure 6, the discrepancy is a constant and does not depend on the presence of the background field, which shows the independence from the global property. Figure 8(a) also supports the localization of the deficit near the boundary.

Another possibility to remedy this defect is to replace the boundary fermion fields (37) to the following extended boundary fields;

$$\begin{aligned} \zeta(\mathbf{n}) &= U_4(n - 2 \cdot \hat{4})U_4(n - \hat{4})P_- \psi(n)|_{n_4=2}, \\ \zeta'(\mathbf{n}) &= U_4(n + \hat{4})^\dagger U_4(n)^\dagger P_+ \psi(n)|_{n_4=N_T-2}, \\ \bar{\zeta}(\mathbf{n}) &= \bar{\psi}(n)P_+U_4(n - \hat{4})^\dagger U_4(n - 2 \cdot \hat{4})^\dagger|_{n_4=2}, \\ \bar{\zeta}'(\mathbf{n}) &= \bar{\psi}(n)P_-U_4(n)U_4(n + \hat{4})|_{n_4=N_T-2}. \end{aligned} \quad (40)$$

In this case the boundary-bulk correlation function becomes

$$\overline{\psi(n)\zeta(\mathbf{m})} = S(n, m)P_+U_4^\dagger(m - \hat{4})U_4^\dagger(m - 2 \cdot \hat{4})\Big|_{m_4=2}, \quad (41)$$

by which we exclude the propagators  $S$  touching the time surface slices at  $n_4 = 1$  and  $N_T - 1$ . This is an explicit solution to remove the deficit that we encountered at the tree-level as far as the deficit is localized at the boundaries because the renormalization constant  $Z_\zeta$  is unity in this case. We will use these boundary to bulk propagators, Eqs. (38) and (41), in the next subsection for the  $O(a)$ -improvement via the PCAC relation.

### 5.3. Tuning on the boundary coefficient $c_{\text{SF}}$

The boundary operator in Eq. (25) causes an  $O(a)$  error in the spectrum. Following Refs. 38, 39 and 40, we employed the PCAC relation to remove the error by tuning the boundary coefficient  $c_{\text{SF}}$ .

In the continuum, the two-point correlation functions used for the PCAC relation are defined by

$$f_A(x_4) = -\frac{1}{(N_f^2 - 1)L^3} \sum_{a=1}^{N_f^2-1} \int d^3\mathbf{x} d^3\mathbf{y} d^3\mathbf{z} \langle A_4^a(x) O^a(\mathbf{y}, \mathbf{z}) \rangle, \quad (42)$$

$$f_P(x_4) = -\frac{1}{(N_f^2 - 1)L^3} \sum_{a=1}^{N_f^2-1} \int d^3\mathbf{x} d^3\mathbf{y} d^3\mathbf{z} \langle P^a(x) O^a(\mathbf{y}, \mathbf{z}) \rangle, \quad (43)$$

$$\begin{aligned} A_\mu^a(x) &= \bar{\psi}(x) \gamma_\mu \gamma_5 T^a \psi(x), & P^a(x) &= \bar{\psi}(x) \gamma_5 T^a \psi(x), \\ O^a(\mathbf{y}, \mathbf{z}) &= \bar{\zeta}(\mathbf{y}) P_+ \gamma_5 T^a P_- \zeta(\mathbf{z}), \end{aligned} \quad (44)$$

where  $T^a$  is the generators of  $\text{SU}(N_f)$  flavor symmetry. The two-point functions with vanishing background field in the continuum theory at the tree-level become

$$f_A(x_4) = -\frac{N_c}{R^2} [E^2 - m^2 + m\{m \cosh(2E(T - x_4)) + E \sinh(2E(T - x_4))\}], \quad (45)$$

$$f_P(x_4) = \frac{N_c E}{R^2} [E \cosh(2E(T - x_4)) + m \sinh(2E(T - x_4))], \quad (46)$$

$$R = E \cosh(ET) + m \sinh(ET), \quad E = \sqrt{\mathbf{p}_0^2 + m^2}, \quad \mathbf{p}_0 = (\theta, \theta, \theta)/L, \quad (47)$$

where  $N_c$  is the number of colors. The ratio at  $x_4 = T/2$  and  $T = 2L$  with  $m = 0$  then becomes

$$\frac{f_A(T/2)}{f_P(T/2)} = -\frac{1}{\cosh(2\sqrt{3}\theta)}. \quad (48)$$

Using the lattice operator  $D_q$  and the boundary fields Eq. (37) including the renormalization constant  $Z_\zeta$  via Eq. (39), the two-point functions on the lattice are given by

$$f_A(n_4) = \frac{-1}{2N_S^3} \text{Tr} \left[ [\tilde{S}(n_4, 1) P_+]^\dagger \gamma_4 [\tilde{S}(n_4, 1) P_+] \right] Z_\zeta^2, \quad (49)$$

$$f_P(n_4) = \frac{1}{2N_S^3} \text{Tr} \left[ [\tilde{S}(n_4, 1) P_+]^\dagger [\tilde{S}(n_4, 1) P_+] \right] Z_\zeta^2, \quad (50)$$

where  $\tilde{S}(n_4, m_4)$  is the zero-momentum projection of  $S(n, m) = (D_q)^{-1}(n, m)$ . At the tree-level, we set  $U_4(n) = 1$ .

The tuning on  $c_{\text{SF}}$  is carried out by fitting  $f_A(T/2)/f_P(T/2)$  as a polynomial function of  $c_{\text{SF}}$  and  $a/L$  and eliminating the  $O(a/L)$  term by tuning  $c_{\text{SF}}$ . The boundary field renormalization  $Z_\zeta$  is not required in the ratio as it cancels out. We

Table 2. Optimal values for  $c_{\text{SF}}$ .

$b_j, c_j$	$b_j = 1, c_j = 0$	$b_j = c_j = 1$	$b_j + c_j = w_j, b_j - c_j = 1$			$b_j = c_j = w_j$		
$m_0$	1.5	1.5	1.0			1.0		
$N_5$	32	32	8	16	32	8	16	32
$c_{\text{SF}}$	0.520	0.312	0.820	0.630	0.5432	0.553	0.392	0.265

fit  $f_A(T/2)/f_P(T/2)$  with

$$\begin{aligned}
f_A(T/2)/f_P(T/2) = & A_{00} + (A_{01} + A_{11}c_{\text{SF}} + A_{21}c_{\text{SF}}^2 + A_{31}c_{\text{SF}}^3)(a/L) \\
& + (A_{02} + A_{12}c_{\text{SF}} + A_{22}c_{\text{SF}}^2 + A_{32}c_{\text{SF}}^3)(a/L)^2 \\
& + (A_{03} + A_{13}c_{\text{SF}} + A_{23}c_{\text{SF}}^2 + A_{33}c_{\text{SF}}^3)(a/L)^3 + \dots \quad (51)
\end{aligned}$$

$A_{00}$  can be fixed to its continuum value using Eq. (48) when there is no background field. The optimal value of  $c_{\text{SF}}$  is thus obtained by solving

$$A_{01} + A_{11}c_{\text{SF}} + A_{21}c_{\text{SF}}^2 + A_{31}c_{\text{SF}}^3 = 0. \quad (52)$$

Table 2 shows the tuning results for several types of MDWF with the tuning performed without the background field. The quasi-optimal parameters used for  $b_j + c_j = w_j, b_j - c_j = 1$  (Optimal Shamir) and  $b_j = c_j = w_j$  (Optimal Chiu) are listed in Table A1 in Appendix A.

To see the effect of the tuning on the  $c_{\text{SF}}$ , we show the relative discrepancy of the ratio  $f_A(n_4)/f_P(n_4)$  between the continuum theory and the lattice theory for the Boriçi domain wall fermion in Figure 9. The left figure (9(a)) is plotted with  $c_{\text{SF}} = 1$ , while the right (9(b)) is plotted using the tuned parameter  $c_{\text{SF}} = 0.312$ . In both cases, the discrepancy vanishes in the continuum limit ( $N_S \rightarrow \infty$ ). This also shows that the surface field renormalization is simply a constant and does not affect the bulk region. The rate of the convergence is faster for the tuned case (right figure). To see the convergence rate more explicitly, we plot the discrepancy at  $t = T/2$  in Figure 10 as a function of  $1/N_T^2 = (a/T)^2$ . With the tuned coefficient, the convergence rate is  $O(a^2)$  (Fig. 10(b)). We also observed a similar behavior for other types of the MDWF, including those with the quasi-optimal coefficients for  $(b_j, c_j)$  from the Zolotarev approximation.

From the observations made in this section, we can conclude that the MDWF with the SF boundary term in Eq. (25) properly reproduces the continuum theory in the most bulk regions through the inclusion of the renormalization at the tree-level.

Using the boundary fields defined in Eq. (40) renormalized with Eq. (39), we can tune  $c_{\text{SF}}$  similarly. The two point functions with Eq. (41) are

$$f_A(n_4) = \frac{-1}{2N_S^3} \text{Tr} \left[ [\tilde{S}(n_4, 2)P_+]^\dagger \gamma_4 [\tilde{S}(n_4, 2)P_+] \right] Z_\zeta^2, \quad (53)$$

$$f_P(n_4) = \frac{1}{2N_S^3} \text{Tr} \left[ [\tilde{S}(n_4, 2)P_+]^\dagger [\tilde{S}(n_4, 2)P_+] \right] Z_\zeta^2, \quad (54)$$

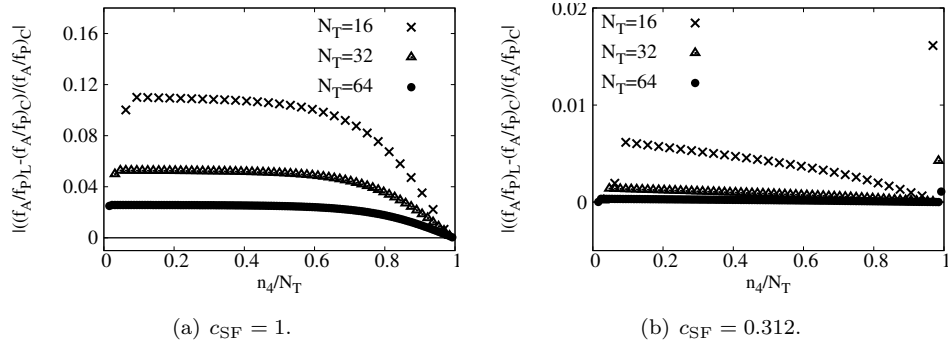
20 *Yuko Murakami and Ken-Ichi Ishikawa*


Fig. 9. Time dependence of the discrepancy of  $f_A(n_4)/f_P(n_4)$  between the continuum and lattice theories. Boriçi domain wall fermion ( $b_j = c_j = 1$ ) with  $N_5 = 16$  is compared.

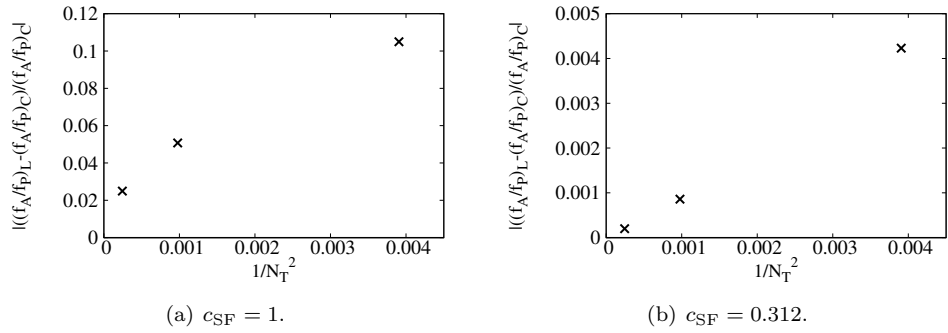


Fig. 10.  $1/N_T^2$  dependence of the discrepancy of  $f_A(N_T/2)/f_P(N_T/2)$  between the continuum and lattice theories. Boriçi domain wall fermion ( $b_j = c_j = 1$ ) with  $N_5 = 16$  is compared.

where the initial time slice of propagators is changed to  $n_4 = 2$  from  $n_4 = 1$  of Eqs. (49) and (50). We find that  $c_{\text{SF}}$  with Eqs. (53) and (54) is almost the same values as listed in Table 2 and the discrepancies are only in the last digit.

With Eq. (41), there is no the boundary renormalization as  $Z_\zeta = 1$ . We also perform the tuning of  $c_{\text{SF}}$  using either  $f_A(n_4)$  (53) or  $f_P(n_4)$  (54), independently. This method also yields identical values for  $c_{\text{SF}}$  to that obtained with fitting the ratio  $f_A/f_P$ .

## 6. Fermionic contribution to the one-loop beta function

The renormalized coupling constant in the SF scheme  $g_{\text{SF}}$  is defined by

$$\frac{1}{g_{\text{SF}}^2} = \frac{1}{k} \frac{\partial \Gamma}{\partial \eta} \Big|_{\eta=0}, \quad (55)$$

$$\Gamma = -\log Z(\eta), \quad (56)$$

$$Z(\eta) = \int \mathcal{D}U \mathcal{D}\bar{\psi} \mathcal{D}\psi \Psi_i[U, \bar{\psi}, \psi, \eta]^* \Psi_f[U, \bar{\psi}, \psi, \eta] e^{-S_g[U] - S_q[U, \bar{\psi}, \psi]}, \quad (57)$$

where  $Z(\eta)$  is the partition function, and  $\Psi_i$  and  $\Psi_f$  are the initial ( $n_4 = 0$ ) and final ( $n_4 = N_T$ ) wave-functionals, respectively. The spatial gauge field at  $n_4 = 0$  and  $n_4 = N_T$  is fixed according to Eq. (28) by the delta wave-functionals contained in  $\Psi_i$  and  $\Psi_f$ , respectively. As seen in Eqs. (28) and (29),  $\eta$  parametrizes the SF boundary condition.  $S_g$  is a lattice gauge action which has Eq. (27) as the classical solution, and  $S_q$  is a fermion action.  $k$  is a normalization constant depending on the gauge action  $S_g$  and is determined to satisfy  $g_{\text{SF}} = g_0$  at the tree-level.

We employ the MDWF action defined in Eq. (8) with the operator Eq. (24) for  $S_q$  by introducing the five-dimensional fermion field  $\Psi$  together with the Pauli-Villars field  $\Phi$ . Using the coupling expansion and the saddle-point approximation, the effective action  $\Gamma$  is expanded as

$$\Gamma = \frac{1}{g_0^2} \Gamma^{(0)} + \Gamma^{(1)} + \dots \quad (58)$$

We focus on the fermionic contribution to  $\Gamma^{(1)}$ . The one-loop contribution to  $g_{\text{SF}}$  is parametrized as

$$g_{\text{SF}}^2 = g_0^2 + p_1 g_0^4 + \dots, \quad p_1 = p_{1,0} + N_f p_{1,1}, \quad (59)$$

where  $N_f$  is the number of flavors included to tag the fermionic contribution  $p_{1,1}$ .

The one-loop coefficient,  $p_{1,1}$ , can be evaluated via

$$p_{1,1} = \frac{1}{k} \sum_{\mathbf{p}} \text{Tr} \left[ \frac{\partial \tilde{D}_{\text{MDWF}}^{(N_5)}}{\partial \eta} \left( \tilde{D}_{\text{MDWF}}^{(N_5)} \right)^{-1} - \frac{\partial \tilde{D}_{\text{PV}}^{(N_5)}}{\partial \eta} \left( \tilde{D}_{\text{PV}}^{(N_5)} \right)^{-1} \right] \Big|_{\eta=0}, \quad (60)$$

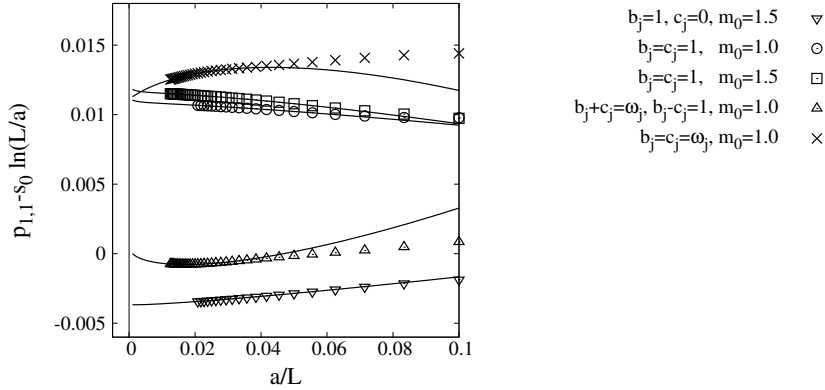
where the summation on  $\mathbf{p}$  is done using the discrete momenta  $\mathbf{p} = (2\pi\mathbf{n} + \theta)/N_S$ ,  $n_k = 0, 1, \dots, N_S - 1$ .  $\tilde{D}_{\text{MDWF}}^{(N_5)}$  and  $\tilde{D}_{\text{PV}}^{(N_5)}$  are the spatial momentum projection of  $D_{\text{MDWF}}^{(N_5)}$  and  $D_{\text{PV}}^{(N_5)}$ , respectively. The trace is over the color, spin, temporal lattice, and fifth-direction lattice indices, and the asymptotic form in  $a \rightarrow 0$  is expected to be

$$p_{1,1} \sim \sum_{k=0}^{\infty} [r_k + s_k \ln(L/a)] (a/L)^k. \quad (61)$$

To validate our construction of the MDWFs for the SF scheme at the one-loop level, we check the following two required conditions: (i)  $s_0$  should coincide with the one-loop beta function  $s_0 = 2b_{0,1} = -1/(12\pi^2) \simeq -0.00844343 \dots$ ; (ii)  $r_0$  should

Table 3. The parameter set used for  $p_{1,1}$  in Eq. (60).

$(b_j, c_j)$	$m_0$	$N_5$	$m_{cr}$	$c_{SF}$	lattice sizes $L/a$
(1, 0)	1.5	8	-0.0039062500	0.520	[4 : 48]
		16	-0.0000152588		[4 : 48]
		32	-0.0000000002		[4 : 48]
(1, 1)	1.0	8, 16, 32	0.0	0.4167	[4 : 48]
	1.5	8	-0.0000025600	0.312	[4 : 80]
		16, 32	0.0		[4 : 48]
$b_j + c_j = w_j$ $b_j - c_j = 1$	1.0	8	-0.0475081142	0.820	[4 : 80]
		16	-0.0003037107	0.630	[4 : 48]
		32	-0.0000000216	0.5432	[4 : 48]
$(w_j, w_j)$	1.0	8	-0.0034031673	0.553	[4 : 72]
		16	-0.0000393319	0.392	[4 : 72]
		32	-0.0000000029	0.265	[4 : 48]

Fig. 11.  $p_{1,1} - s_0 \ln(L/a)$  as a function of  $a/L$  with  $N_5 = 8$ . The solid lines are the fit results obtained in Table 4.

reproduce the known universal relation of the running coupling constant between the SF and  $\overline{MS}$  schemes. The terms  $r_1$  and  $s_1$  correspond to the  $O(a)$  discretization errors; whereas  $r_1$  can be eliminated by  $c_t$ , the coefficient of the temporal boundary term of the gauge action.<sup>15, 17, 39, 40, 62</sup>  $s_1$  must be absorbed by the counter terms in the fermion action. When the lattice chiral symmetry in the bulk region is exact, the  $O(a)$  error is induced only by the temporal boundary effect. In this case, the error can be removed solely by  $c_{SF}$ . At a small  $N_5$ , where the lattice chiral symmetry in the bulk region is violated, another term similar to the clover term in the bulk region is necessary to remove the  $O(a)$  error of  $s_1$ . Therefore, monitoring  $s_1$  provides a test for chiral symmetry.

We numerically evaluated Eq. (60) with  $N_S = N_T$  using the parameters shown in Table 3 by varying the lattice sizes in steps of two over the given range. For the optimal type domain wall fermions, we used the quasi-optimal coefficients  $(b_j, c_j)$

Table 4. Best fit results of  $p_{1,1}$  with Eq. (61) for each MDWF at  $N_5 = 8$ .

$(b_j, c_j)$	$b_j = 1, c_j = 0$	$b_j = c_j = 1$		$b_j + c_j = w_j,$ $b_j - c_j = 1$	$b_j = c_j = w_j$
$m_0$	1.5	1.0	1.5	1.0	1.0
Fit range	$18 \leq L/a \leq 48$	$18 \leq L/a \leq 48$	$16 \leq L/a \leq 80$	$38 \leq L/a \leq 80$	$32 \leq L/a \leq 72$
$r_0$	-0.003760(57)	0.01015(24)	0.01056(19)	-0.00085(30)	0.01033(94)
$s_0$	-0.008430(11)	-0.008318(44)	-0.008268(33)	-0.008299(50)	-0.00835(16)
$r_1$	0.03151(41)	-0.0321(17)	-0.0504(18)	0.1269(55)	-0.132(14)
$s_1$	-0.00474(31)	0.0087(13)	0.0149(12)	-0.0386(28)	0.0623(76)
$\chi^2/\text{d.o.f}$	$1.48 \times 10^{-7}$	$6.11 \times 10^{-7}$	$2.67 \times 10^{-6}$	$3.46 \times 10^{-7}$	$1.40 \times 10^{-6}$

shown in Table A1 in Appendix A. The approximation range was fixed to  $x \in [0.001 : 1.00]$  for the optimal Shamir domain wall fermion ( $b_j + c_j = w_j, b_j - c_j = 1$ ), and  $x \in [0.01 : 7.00]$  for the optimal Chiu domain wall fermion ( $b_j = c_j = w_j$ ). As the largest lattice sizes for the optimal type MDWF's satisfy the approximation boundary conditions in Eqs. (31) and (32), the continuum limit could be taken safely without spoiling the signum function approximation. All numerically evaluated values for  $p_{1,1}$  are tabulated in Appendix B.

We first validated the one-loop beta function  $s_0$  by fitting  $p_{1,1}$  as a function of  $1/N_S$  assuming the asymptotic form (61) including up to  $O((a/L)^2)$  terms. All  $r_k$  and  $s_k$  were taken as free parameters to validate the one-loop beta function  $s_0$ . We varied the cut-off  $a/L = 1/N_S$  of the fit range  $[0 : a/L]$  and the maximum order of the fitting function and investigated the stability on the fit result for  $s_0$  to examine the consistency. Figure 11 shows the cut-off  $a/L$  dependence of  $p_{1,1} + (1/12\pi^2) \ln(L/a)$  with  $N_5 = 8$  as an example of the fitting. The solid lines are the best fits obtained in the stability analysis and corresponding coefficients are listed in Table 4, where functions including up to  $O(a/L)$  terms yields the best fit. As seen in the figure and values in the table, the optimal Chiu type ( $b_j = c_j = w_j$ : crosses) and the optimal Shamir type ( $b_j + c_j = w_j, b_j - c_j = 1$ : up-triangles) have large values for  $s_1$  ( $O(a \log(a))$  term), which indicates that these actions have a less stability on  $s_0$  in the fit range analysis. We observed the stability in an asymptotic region, confirming that  $s_0$  is consistent with the universal one-loop beta function within 10% accuracy with most of the tested MDWF actions, with the exception of the optimal Chiu type ( $b_j = c_j = w_j$ ), for which the discrepancy with  $N_5 = 8$  was 20%.

We believe that the discrepancy with the optimal Chiu domain wall fermion with  $N_5 = 8$  can be explained as follows. We employed  $x \in [0.01 : 7.0]$  as the approximation range for the quasi-optimal coefficient  $b_j$  for the overlap type kernel  $\mathcal{H}_W = \gamma_5 D_W$ . The spectrum of this overlap kernel behaves as in Eq. (32), and limiting the largest lattice size to  $N_S = 72$ . This case has a large  $O(a)$  error from explicit chiral symmetry breaking and, therefore, asymptotic behavior to extract the logarithmic cut-off dependence is not captured within the narrow fit range. To extend the fit range towards the asymptotic region in  $a/L \rightarrow 0$ , it is necessary to

decrease the lower limit of the approximation range. For the optimal Chiu MDWF cases with  $N_5 = 16$  and  $32$ , the effect of the explicit chiral symmetry breaking is suppressed, and therefore the logarithmic divergence is captured in the fit ranges we examined.

We then investigated  $r_0$  in terms of the universal relation of the running coupling constants between the SF and  $\overline{\text{MS}}$  schemes.<sup>a</sup> The one-loop relation between the two schemes is known<sup>17,62</sup> to be given by

$$\alpha_{\overline{\text{MS}}}(\mu) = \alpha_{\text{SF}}(\mu) [1 + c_1 \alpha_{\text{SF}}(\mu) + \dots], \quad \mu = 1/L, \quad (62)$$

$$c_1 = c_{1,0} + N_f c_{1,1}, \quad (63)$$

$$c_{1,0} = 1.25563(4), \quad c_{1,1} = \begin{cases} 0.039863(2) & \text{for } \theta = \pi/5 \\ 0.022504(2) & \text{for } \theta = 0 \end{cases}, \quad (64)$$

where  $c_{1,0}$  is the gluonic contribution<sup>17</sup> and  $c_{1,1}$  is the fermionic contribution.<sup>62</sup> This relation is universal and independent of the regularization used in the SF scheme. We employ the lattice regularization with the MDWF in the SF scheme and employ the one-loop relation between the lattice bare coupling and the coupling renormalized with the SF scheme as in Eq. (59). To extract  $c_{1,1}$  from  $r_0$ , it is necessary to know the one-loop relation between the lattice bare coupling with the MDWF and the coupling renormalized with the  $\overline{\text{MS}}$  scheme.

The MDWF action with  $b_j + c_j = w_j, b_j - c_j = 1$  (optimal Shamir domain wall fermion) is equivalent to the standard domain wall fermion action in the infinite size of  $N_5$ . Therefore,  $r_0$  is expected to have a common value between the lattice fermions at  $N_5 = \infty$ . The one-loop relation between the lattice bare coupling with the standard domain wall fermion at  $N_5 = \infty$  and  $\alpha_{\overline{\text{MS}}}$  was previously obtained in Ref. 65; by combining these results with the universal relation (62), we expect  $r_0 = 0.0010886(51)$  at  $am_0 = 1.0$  and  $r_0 = -0.0026362(33)$  at  $am_0 = 1.5$  in  $N_5 \rightarrow \infty$  for the optimal Shamir domain wall fermion.

Similarly, the optimal Chiu ( $b_j = c_j = w_j$ ) and Borici ( $b_j = c_j = 1$ ) DWFs at  $N_5 = \infty$  are equivalent to the overlap fermion action, and  $r_0$  is expected to have the same value as that derived from the overlap fermion. In Appendix C, we show the equivalence of  $p_{1,1}$  between the MDWF theory of Eq. (8) and the truncated overlap fermion theory (18) defined with the same operator (24) at a finite  $N_5$  algebraically. Using the one-loop relation between the lattice bare coupling with the overlap fermion and  $\alpha_{\overline{\text{MS}}}$  obtained in Ref. 66, we expect  $r_0 = 0.01118458(16)$  at  $am_0 = 1.0$  and  $r_0 = 0.01191070(16)$  at  $am_0 = 1.5$  for the MDWF with  $b_j = c_j$  at  $N_5 = \infty$ .

We fit  $p_{1,1}$  with Eq. (61) by fixing  $s_0 = -1/(12\pi^2)$  to extract  $r_0$ . We excluded the optimal Chiu DWF with  $N_5 = 8$  from the analysis, as we failed the validation on  $s_0$  in the fit analysis without constraints. We employed three fit functions to

<sup>a</sup>The value of  $r_0$  itself depends on the lattice action and is not universal because it is computed with lattice regularization in the bare coupling expansion. We employ the universal relation of the running coupling constants between the SF and  $\overline{\text{MS}}$  schemes to validate  $r_0$ .

Table 5. Fit results for  $r_0$  with  $s_0$  is fixed at  $-1/(12\pi^2)$ . The values in the bottom row ( $N_5 = \infty$ ) are estimated from the universal relation between the couplings in the SF and  $\overline{\text{MS}}$  schemes, and the relation between the coupling in the  $\overline{\text{MS}}$  scheme and lattice bare coupling scheme with the standard domain wall fermion at  $N_5 = \infty$  and the overlap fermion.

$m_0$	1.0			1.5	
$N_5$	$b_j + c_j = w_j,$ $b_j - c_j = 1$	$b_j = c_j = 1$	$b_j = c_j = w_j$	$b_j = 1, c_j = 0$	$b_j = c_j = 1$
8	-0.00100(18)	0.010952(9)	-	-0.00373594(6)	0.011679(5)
16	0.001076(15)	0.01116(3)	0.01103(15)	-0.0026696(16)	0.01184(15)
32	-	0.01116(4)	0.0111661(18)	-0.002634(2)	0.01181(4)
$\infty$	0.0010886(51)	0.01118458(16)		-0.0026362(33)	0.01191070(16)

Table 6. Fit results for  $s_1$ .  $s_0$  is fixed at  $-1/(12\pi^2)$  and  $r_0$  are fixed at the universal values at  $N_5 = \infty$ .

$m_0$	1.0			1.5	
$N_5$	$b_j + c_j = w_j,$ $b_j - c_j = 1$	$b_j = c_j = 1$	$b_j = c_j = w_j$	$b_j = 1, c_j = 0$	$b_j = c_j = 1$
16	-0.00115(3)	0.00116(6)	-0.0080(7)	-	0.0041(13)
32	-	0.00112(4)	-0.00490(3)	-0.0014(2)	0.0038(9)

estimate  $r_0$ ,

$$f(x) = r_0^f + s_0 \ln(x) + (r_1^f + s_1^f \ln(x))/x, \quad (65)$$

$$p(x) = r_0^p + s_0 \ln(x) + (r_1^p + s_1^p \ln(x))/x + (r_2^p + s_2^p \ln(x))/x^2, \quad (66)$$

$$r(x) = r_0^r + s_0 \ln(x) + (r_1^r + s_1^r \ln(x))/x + (r_2^r + s_2^r \ln(x))/x^2 + (r_3^r + s_3^r \ln(x))/x^3, \quad (67)$$

where  $x = L/a$ . Table 5 shows the fit results for  $r_0$ , in which the error is estimated from the stability on the fit results by varying the fit range and changing the fitting function. We confirm that the values of  $r_0$  all agree with the expected values for sufficiently large  $N_5$ . From these observations on  $s_0$  and  $r_0$ , we conclude that the MDWF with the boundary term in Eq. (25) actually satisfies the desired universality at  $N_5 = \infty$ .

To validate  $r_0$  at a small  $N_5$ , an independent computation of the one-loop relation between the lattice bare coupling and the coupling in the  $\overline{\text{MS}}$  scheme with the MDWF at the small  $N_5$  is required as in Refs. 65, 66.

We also investigated the effect of lattice chiral symmetry on the  $O(a)$  error and the  $O(a)$ -improvement through the adjustment of the boundary coefficient  $c_{\text{SF}}$ . For this purpose, we evaluated  $r_1$  and  $s_1$ . After investigating  $r_1$  and  $s_1$ , the lattice artifact on the lattice step-scaling function<sup>67</sup> will be discussed. As mentioned previously, the  $O(a)$  error of  $r_1$  is absorbed by the boundary counter term of the gauge action,<sup>25, 40</sup> while that of  $s_1$  can be removed by the boundary coefficient  $c_{\text{SF}}$  when

Table 7. Fit results for  $r_1$ .  $s_0$  is fixed at  $-1/(12\pi^2)$  and  $r_0$  are at the universal values at  $N_5 = \infty$ .

$m_0$	1.0		1.5
$(b_j, c_j)$	$b_j + c_j = w_j,$ $b_j - c_j = 1$	$b_j = c_j = 1$	$b_j = 1, c_j = 0$
$N_5$	16	32	32
$r_1$	0.014(20)	-0.018(12)	0.01409(62)

the lattice chiral symmetry in the bulk region is exact. We fit  $p_{1,1}$  with

$$f(x) = r_0 + s_0 \ln(x) + (r_1^f + s_1^f \ln(x))/x, \quad (68)$$

$$p(x) = r_0 + s_0 \ln(x) + (r_1^p + s_1^p \ln(x))/x + (r_2^p + s_2^p \ln(x))/x^2, \quad (69)$$

where  $s_0$  and  $r_0$  are fixed to the universal values to make the effect of the  $O(a)$ -improvement by  $c_{\text{SF}}$  apparent. The error on  $s_1$  was estimated in the same manner as that of  $r_0$ . Table 6 shows the fit results for  $s_1$ , which would be expected to be zero when  $N_5$  is effectively infinite and  $c_{\text{SF}}$  is properly tuned; as is seen, the values of  $s_1$  are close to, but slightly deviating from, zero. This deviation can arise from a remaining explicit lattice chiral symmetry breaking at finite  $N_5$  or a miss-tuning of  $c_{\text{SF}}$ . To confirm the  $O(a)$ -improvement more precisely, more  $p_{1,1}$  data at larger  $L/a$  will be needed to stabilize the fitting to the asymptotic form.

Table 7 shows the fit results for  $r_1$ , where the coefficients  $r_0, s_0$  and  $s_1$  are fixed as  $r_0 = \text{universal values at } N_5 = \infty, s_0 = 2b_{0,1}, s_1 = 0$ . Since actions with  $b_j = c_j = w_j, m_0 = 1.0, N_5 = 32$  (Optimal Chiu) and  $b_j = c_j = 1, m_0 = 1.5, N_5 = 32$  (Borici) show slightly larger values for  $s_1$  as seen in Table 6,  $r_1$  had large errors and could not be determined with the stability analysis. For other actions,  $r_1$  could be determined with regardless of the constraint of  $s_1 = 0$  though large uncertainty remains.

We investigated the lattice cut-off error of the step-scaling function<sup>67</sup> in the SF scheme. The step-scaling function  $\sigma(2, u)$  with the scaling factor 2 is defined by

$$\sigma(2, u) = g_{\text{SF}}^2(2L), \quad u = g_{\text{SF}}^2(L). \quad (70)$$

The lattice version of the step-scaling function at a finite cut-off  $a$  is

$$\Sigma(2, u, a/L) = g_{\text{SF}}^2(2L, a), \quad u = g_{\text{SF}}^2(L, a). \quad (71)$$

The discretization error of the lattice step-scaling function is analyzed through

$$\delta(2, L, a) \equiv \frac{\Sigma(2, u, a/L) - \sigma(2, u)}{\sigma(2, u)}. \quad (72)$$

The perturbative expansion of the discretization error in terms of the coupling constant  $u$  becomes

$$\delta(2, L, a) = \delta_1(a/L)u + O(u^2), \quad (73)$$

where the one-loop coefficient  $\delta_1(a/L)$  involves pure gauge part and fermionic part,<sup>62</sup>

$$\delta_1(a/L) = \delta_{1,0}(a/L) + N_f \delta_{1,1}(a/L). \quad (74)$$

Using Eq. (59), the discretization error of the fermionic part is given by

$$\delta_{1,1}(a/L) = p_{1,1}(2L/a) - p_{1,1}(L/a) - (2b_{0,1}) \log(2). \quad (75)$$

The cut-off dependence of Eq. (75) can be parametrized via the asymptotic form of Eq. (61). The terms with coefficients  $r_1$  and  $s_1$  in the asymptotic expansion correspond to the  $O(a)$  error of the step-scaling function, and terms with  $r_1$  can be removed by absorbing it to  $c_t$ .<sup>15, 17, 39, 40, 62</sup> We also investigated the  $O(a)$ -improved version of Eq. (75) defined by

$$\delta_{1,1}^{(1)}(a/L) = p_{1,1}(2L/a) - p_{1,1}(L/a) - (2b_{0,1}) \log(2) + \frac{r_1}{2} \left( \frac{a}{L} \right), \quad (76)$$

for actions listed in Table 7. To clarify the  $O(a)$ -improvement via  $c_t$ , we use the symbol  $\delta_{1,1}^{(0)}(a/L) = \delta_{1,1}(a/L)$  for the unimproved version.

Figure 12 shows the cut-off  $a/L$  dependence of  $\delta_{1,1}^{(0)}(a/L)$ . Wilson and Clover fermions are included for comparison.<sup>62</sup> <sup>b</sup> The Clover fermion does not include the boundary  $O(a)$ -improvement of removing  $r_1$  in Fig. 12. Borici type actions (dash-dot and long-dash lines) and Shamir type action with  $am_0 = 1.5$  (dash line) show non-monotonic behaviors. The magnitude of  $\delta_{1,1}^{(0)}(a/L)$  is comparable among actions we investigated. The size is smaller than that of Wilson action (three-dashed line) and Clover action (solid line) except for Borici action with  $m_0 = 1.5, N_5 = 32$  (dash-dot line). Figure 13 shows the cut-off  $a/L$  dependence of  $\delta_{1,1}^{(1)}(a/L)$  after the  $O(a)$ -improvement removing  $r_1$ , where central values in Table 7 are used for  $r_1$ . Although errors are significantly reduced by the  $O(a)$ -improvement in the region  $a/L < 1/10$ , errors in  $a/L > 1/10$  are larger than that of Clover fermion (solid line,  $r_1$  is removed) and Shamir type with  $m_0 = 1.0, N_5 = 16$  (dot line) actions. It seems that the large errors in  $a/L > 1/10$  are caused by the non-monotonic behaviors seen in the unimproved version.

## 7. Conclusion

We constructed the appropriate boundary operator for the MDWFs needed to define the SF scheme by extending Takeda's standard domain wall fermion formulation.

We investigated the effective four-dimensional operator derived from the MDWF at the tree-level and confirmed that its spectrum and propagator reproduce the continuum behavior in the continuum limit, except for the boundary surfaces, where the normalization of the propagator differs by a constant from that of the continuum theory.

We proposed two solutions to cure the deficit in the propagator. One solution is to absorb the discrepancy into the renormalization of the boundary fields defined

<sup>b</sup>We have reproduced the data and have checked the consistency with that of Ref. 62.

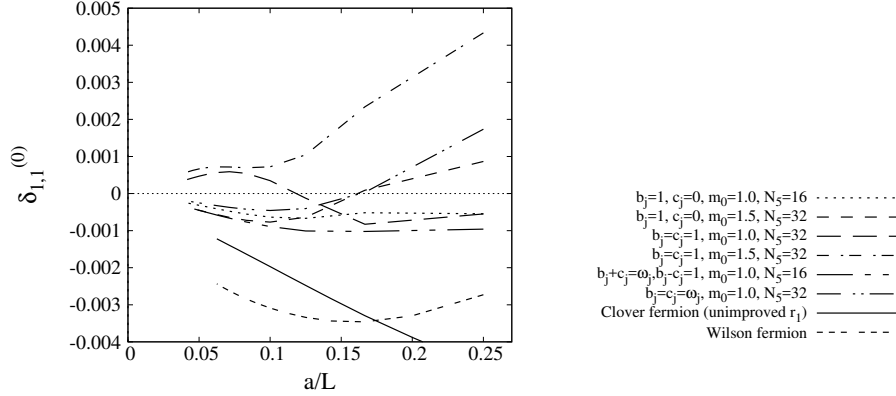
28 *Yuko Murakami and Ken-Ichi Ishikawa*


Fig. 12.  $\delta_{1,1}^{(0)}$  as a function of  $a/L$ . Dot line ( $b_j = 1, c_j = 0, m_0 = 1.0, N_5 = 16$ ) is taken from Ref. 40 and solid (Clover) and three-dashed (Wilson) lines are reproduced with Ref. 62.

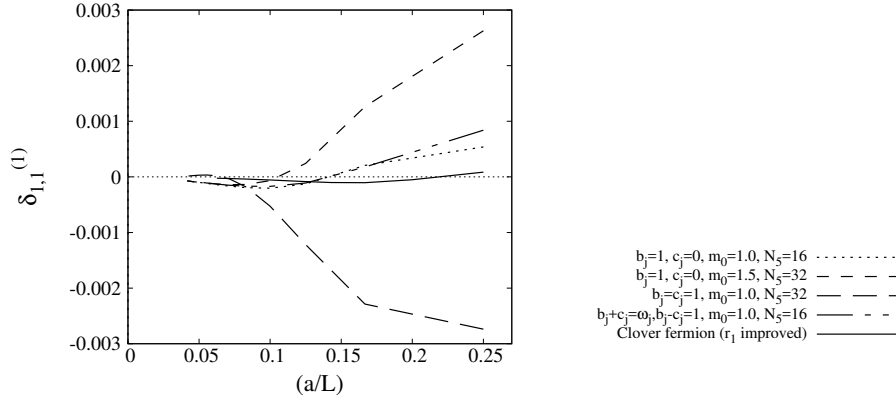


Fig. 13.  $\delta_{1,1}^{(1)}$  as a function of  $a/L$ .

in a form usually seen the literature. We found that the discrepancy is independent from the presence of the background field, which satisfies a required condition of the renormalization via the renormalization of the boundary fields at the tree-level. Another solution is to define the boundary fields that are extended to two time slices in the bulk time region to avoid the surface time slices of the propagator. This works for  $f_A$  and  $f_P$ , and this is the solution to avoid the renormalization.

Using several parameter sets, we investigated the fermionic contribution of the MDWF to the one-loop beta function,  $p_{1,1}$ , and were able to extract the one-loop beta function consistent with the universal value within a 10% difference for most of the sets. The one exception was the case with the optimal Chiu domain wall fermion with  $N_5 = 8$ , which produced a 20% deviation from the universal one-loop

beta function. We also examined the universal relation of the couplings between the SF and  $\overline{\text{MS}}$  and found that the cases with sufficiently larger  $N_5$  were consistent with the known values from the standard domain wall and overlap fermions. To validate the universality of the coupling relation between the SF and  $\overline{\text{MS}}$  schemes with the MDWF at smaller  $N_5$ , another validation using the relation between the  $\overline{\text{MS}}$  and bare lattice couplings with the MDWF will be required. We also investigated the lattice artifact of the lattice step-scaling function at the one-loop level, and found that the size of the lattice artifact is comparable to that of the standard domain wall fermion.

Based on these results, we can conclude that the boundary operator we introduced is one of the realizations of the SF scheme for the Möbius domain wall fermions, at least at larger  $N_5$  or  $N_5 = \infty$ .

### Acknowledgments

We would like to thank S. Takeda for the computational advice and the useful discussion. We thank anonymous referee for his/her helpful comments on the surface field renormalization. The numerical computations have been done on the workstations of the INSAM (Institute for Nonlinear Sciences and Applied Mathematics) at Hiroshima University and on FUJITSU PRIMERGY CX400 (Tatara system) and new FUJITSU PRIMERGY (ITO system) of the Research Institute for Information Technology at Kyushu University. This work was partly supported by JSPS KAKENHI Grant Numbers 24540276 and 16K05326, and Core of Research for the Energetic Universe (CORE-U) at Hiroshima University.

**Appendix A. Tables for quasi-optimal parameters  $b_j$** 

In this appendix, we list the quasi-optimal parameters  $b_j$  for the  $N_5 = 8, 16$  and  $32$  cases. The approximation range is fixed to  $x \in [0.001 : 1.00]$  for the optimal Shamir domain wall fermion (OSDWF,  $b_j + c_j = w_j, b_j - c_j = 1$ ) and  $x \in [0.01 : 7.00]$  for the optimal Chiu domain wall fermion (OCDWF,  $b_j = c_j = w_j$ ). We introduce  $\delta^{N_5} = |1 - R_{N_5}|$  to see the quality of the approximation.

Table A1. The MDWF  $b_j$  parameters.

OSDWF			
$N_5$	8	16	32
$\delta^{N_5}$	$\leq 0.091$	$\leq 0.00061$	$\leq 4.3 \times 10^{-8}$
$j$	$b_j$		
1	1.375560445952	1.070238032009	0.016892137272
2	5.471160816064	1.730342867161	0.158913006904
3	50.79006488628	3.876257791467	0.482041690426
4	286.0314000944	9.868218005280	1.074927835108
5		27.18597163933	2.100739142300
6		74.54647850997	3.840873748406
7		203.6953910351	6.774084261660
8		438.9134097812	11.70429696596
9			19.98458839515
10			33.86858730352
11			57.09209193583
12			95.62651877838
13			158.2374319172
14			254.0716769840
15			378.9127561311
16			483.1599011152

OCDWF			
$N_5$	8	16	32
$\delta^{N_5}$	$\leq 0.072$	$\leq 0.00039$	$\leq 1.8 \times 10^{-8}$
$j$	$b_j$		
1	0.237921110807	0.161123304598	0.147274921719
2	1.265028710883	0.331200294113	0.184266408796
3	11.292798466011	0.862987775592	0.267551476942
4	60.043912191189	2.293352637899	0.418026489555
5		6.229183445073	0.673528275619
6		16.553785221249	1.098151069375
7		43.133157003882	1.798613861602
8		88.663240375751	2.950400432880
9			4.841957764956
10			7.942624367962
11			13.008878909391
12			21.210266595825
13			34.174184274611
14			53.394264344831
15			77.527501507451
16			97.000318309165

**Appendix B. Tables for  $p_{1,1}$** 

In this appendix, we provide tables for the numerical values of  $p_{1,1}$ .

Table B1. The numerical values of  $p_{1,1}$  with  $b_j + c_j = w_j$ ,  $b_j - c_j = 1$ , and  $m_0 = 1.0$ .

$N_5$	8	16
$L/a$	$p_{1,1}$	
4	-0.008078678483014	-0.007549846131326
6	-0.012704626284028	-0.011543790007817
8	-0.016099359107337	-0.014362647277993
10	-0.018603053000762	-0.016601560471003
12	-0.020509350351466	-0.018419096227329
14	-0.022043043374366	-0.019932682101795
16	-0.023334785689534	-0.021224758101492
18	-0.024458027530347	-0.022349705318640
20	-0.025455706039567	-0.023344258955488
22	-0.026354442980561	-0.024234463201614
24	-0.027171888915236	-0.025039552752149
26	-0.027920587948598	-0.025774134656849
28	-0.028610040120546	-0.026449513032584
30	-0.029247813609523	-0.027074562214969
32	-0.029840155519369	-0.027656336722746
34	-0.030392340093947	-0.028200511774470
36	-0.030908880213565	-0.028711707029837
38	-0.031393667187825	-0.029193726826378
40	-0.031850071712519	-0.029649739643784
42	-0.032281022324532	-0.030082412981785
44	-0.032689069460135	-0.030494015386321
46	-0.033076439227606	-0.030886494192633
48	-0.033445079148571	-0.031261535256350
50	-0.033796697257952	
52	-0.034132795554748	
54	-0.034454698597199	
56	-0.034763577918903	
58	-0.035060472857527	
60	-0.035346308315376	
62	-0.035621909905414	
64	-0.035888016875790	
66	-0.036145293150457	
68	-0.036394336774732	
70	-0.036635688010451	
72	-0.036869836288573	
74	-0.037097226193355	
76	-0.037318262626538	
78	-0.037533315274019	
80	-0.037742722480864	

Table B2. The numerical values of  $p_{1,1}$  with  $b_j = c_j = w_j$  and  $m_0 = 1.0$ .

$N_5$	8	16	32
$L/a$	$p_{1,1}$		
4	-0.000427658644074	-0.000383843417187	-0.001367108292250
6	-0.001690115887320	-0.002015195493540	-0.003292843399314
8	-0.003276057963329	-0.004212644775318	-0.005485336972469
10	-0.005033155003610	-0.006246918403858	-0.007449843475257
12	-0.006705005271095	-0.007992466113233	-0.009112723836382
14	-0.008193831514685	-0.009490189069814	-0.010524786720790
16	-0.009494057300111	-0.010790678620702	-0.011742834419345
18	-0.010630559779250	-0.011933438152156	-0.012810419169036
20	-0.011632825706636	-0.012948842121387	-0.013759177135561
22	-0.012526885001577	-0.013860522358465	-0.014612217134086
24	-0.013333735423218	-0.014686861614616	-0.015386734394376
26	-0.014069766215183	-0.015442121609423	-0.016095786578485
28	-0.014747628848984	-0.016137387857025	-0.016749483310047
30	-0.015377075017193	-0.016781345974691	-0.017355791924810
32	-0.015965645179162	-0.017380889556003	-0.017921092828360
34	-0.016519204136393	-0.017941576933597	-0.018450569412746
36	-0.017042349063875	-0.018467964970409	-0.018948486893592
38	-0.017538717989105	-0.018963849305390	-0.019418395305982
40	-0.018011222352760	-0.019432436525828	-0.019863279824302
42	-0.018462222102058	-0.019876468167950	-0.020285673857459
44	-0.018893657364280	-0.020298311160125	-0.020687745384951
46	-0.019307147334419	-0.020700025025448	-0.021071363741383
48	-0.019704064430391	-0.021083412945066	-0.021438151897327
50	-0.020085589825083	-0.021450061496227	
52	-0.020452754991647	-0.021801372306609	
54	-0.020806472777243	-0.022138587806451	
56	-0.021147560664753	-0.022462812558580	
58	-0.021476758226712	-0.022775031183158	
60	-0.021794740276988	-0.023076123590416	
62	-0.022102126845674	-0.023366878034668	
64	-0.022399490814134	-0.023648002369445	
66	-0.022687363830450	-0.023920133794130	
68	-0.022966240962226	-0.024183847319741	
70	-0.023236584421461	-0.024439663137563	

Table B3. The numerical values of  $p_{1,1}$  with  $b_j = 1, c_j = 0$  and  $m_0 = 1.5$ .

$N_5$	8	16	32
$L/a$	$p_{1,1}$		
4	-0.013700543988949	-0.013494117365375	-0.013493847599046
6	-0.0169404256660898	-0.016440093560490	-0.016435046256293
8	-0.019207595711335	-0.018495725966135	-0.018480529959025
10	-0.021308125813259	-0.020479834297536	-0.020459083387075
12	-0.023122800312741	-0.022221285948861	-0.022198883266909
14	-0.024665375229509	-0.023711578334847	-0.023688561490842
16	-0.025987047538505	-0.024995171537818	-0.024971355383199
18	-0.027135213800013	-0.026116105185960	-0.026091198129590
20	-0.028146880041840	-0.027108518882633	-0.027082437011268
22	-0.029049775493944	-0.027997747140651	-0.027970577120069
24	-0.029864559491185	-0.028802679063304	-0.028774578712134
26	-0.030606757871299	-0.029537633821171	-0.029508765297232
28	-0.031288217026821	-0.030213664582947	-0.030184166135890
30	-0.031918135064723	-0.030839449899792	-0.030809430378576
32	-0.032503778953037	-0.031421910597608	-0.031391453294570
34	-0.033050983428172	-0.031966644411249	-0.031935813074617
36	-0.033564501913902	-0.032478237562439	-0.032447081752874
38	-0.034048257349549	-0.032960491706605	-0.032929050814620
40	-0.034505524685294	-0.033416591708052	-0.033384897755921
42	-0.034939066008357	-0.033849231429220	-0.033817310976307
44	-0.035351232253616	-0.034260709315154	-0.034228584756533
46	-0.035744040922304	-0.034653001956654	-0.034620692426401
48	-0.036119236284169	-0.035027821389594	-0.034995343407687

Table B4. The numerical values of  $p_{1,1}$  with  $b_j = c_j = 1$  and  $m_0 = 1.5$ .

$N_5$	8	16	32
$L/a$	$p_{1,1}$		
4	-0.006727819825856	-0.006665138308415	-0.006666313597976
6	-0.007414851979212	-0.007313811347951	-0.007315034976460
8	-0.008380305729795	-0.008194515940394	-0.008185897962635
10	-0.009706986889307	-0.009534951147513	-0.009513426996691
12	-0.010940734313774	-0.010849913953446	-0.010828496014809
14	-0.012005880912213	-0.012000303082120	-0.011989158728680
16	-0.012933090094362	-0.012990681811199	-0.012992846763797
18	-0.013759688673405	-0.013854127110319	-0.013868798328790
20	-0.014511760217989	-0.014620713721791	-0.014645831748636
22	-0.015205517755086	-0.015312808751915	-0.015346126770424
24	-0.015851036926812	-0.015946323963520	-0.015985730259767
26	-0.016454984507842	-0.016532563270011	-0.016576163504983
28	-0.017022194974289	-0.017079658119618	-0.017125805557620
30	-0.017556489774245	-0.017593563907684	-0.017640879135091
32	-0.018061078280186	-0.018078737359153	-0.018126116251055
34	-0.018538749124392	-0.018538597095271	-0.018585202424702
36	-0.018991964014254	-0.018975837134752	-0.019021074631616
38	-0.019422909145805	-0.019392639865905	-0.019436123561516
40	-0.019833529265709	-0.019790820185260	-0.019832332961955
42	-0.020225554783800	-0.020171922778777	-0.020211377175424
44	-0.020600525735608	-0.020537287838630	-0.020574690536960
46	-0.020959813694587	-0.020888095769654	-0.020923517571072
48	-0.021304641794774	-0.021225398065531	-0.021258949911228
50	-0.021636102804375		
52	-0.021955175221099		
54	-0.022262737442725		
56	-0.022559580138765		
58	-0.022846416992679		
60	-0.023123893996791		
62	-0.023392597486309		
64	-0.023653061081057		
66	-0.023905771690838		
68	-0.024151174719892		
70	-0.024389678584948		
72	-0.024621658651276		
74	-0.024847460666186		
76	-0.025067403767381		
78	-0.025281783121781		
80	-0.025490872250634		

Table B5. The numerical values of  $p_{1,1}$  with  $b_j = c_j = 1$  and  $m_0 = 1.0$ .

$N_5$	8	16	32
$L/a$	$p_{1,1}$		
4	-0.000996246152616	-0.000931659891244	-0.000931919758575
6	-0.004603150636507	-0.004379720711230	-0.004377564445862
8	-0.007570846735406	-0.007339903403487	-0.007334795622206
10	-0.009663145567390	-0.009487128771071	-0.009482501467147
12	-0.011187581989197	-0.011061057467551	-0.011058231188890
14	-0.012384896118215	-0.012290534341752	-0.012289409163346
16	-0.013389461252875	-0.013310783001584	-0.013310976363075
18	-0.014270981623373	-0.014195328866723	-0.014196493673909
20	-0.015065582916720	-0.014984779892570	-0.014986622226234
22	-0.015792971302519	-0.015702711408268	-0.015704971170587
24	-0.016465000994347	-0.016363707733056	-0.016366158318439
26	-0.017089703923897	-0.016977430784739	-0.016979889094112
28	-0.017673114155514	-0.017550726401246	-0.017553059566649
30	-0.018220085378664	-0.018088745432749	-0.018090869408541
32	-0.018734670587965	-0.018595557661083	-0.018597429341229
34	-0.019220317416919	-0.019074498753218	-0.019076105281324
36	-0.019679985859805	-0.019528374164715	-0.019529722477420
38	-0.020116231188214	-0.019959585129973	-0.019960693392692
40	-0.020531268659271	-0.020370211346101	-0.020371102773105
42	-0.020927026511223	-0.020762068840545	-0.020762767700268
44	-0.021305190093525	-0.021136752957334	-0.021137282277683
46	-0.021667238733567	-0.021495671861383	-0.021496052316441
48	-0.022014476511803	-0.021840073569361	-0.021840323109700

### Appendix C. Equivalence of the fermionic contribution $p_{1,1}$ between the five-dimensional operator and the effective four-dimensional operator

In this appendix, we prove the equivalence of  $p_{1,1}$  constructed with the MDWF and with the effective four-dimensional operators.

With the MDWF operator in the five-dimensional lattice, the fermionic contribution  $p_{1,1}$  is defined by

$$\begin{aligned}
p_{1,1} &= \frac{1}{k} \frac{\partial}{\partial \eta} \left[ \text{Tr} \ln [Z^{-1} D_{PV}^{-1} D_{\text{MDWF}}] \right] \\
&= \frac{1}{k} \text{Tr} \left[ \frac{\partial D_{\text{MDWF}}}{\partial \eta} (D_{\text{MDWF}})^{-1} - \frac{\partial D_{\text{PV}}}{\partial \eta} (D_{\text{PV}})^{-1} \right]. \quad (\text{C.1})
\end{aligned}$$

The trace is taken on the five-dimensional lattice sites, color, and spinor indices. Eq. (60) is the momentum space representation of Eq. (C.1). In this appendix, we omit the superscript  $N_5$  and substitute  $\eta = 0$  after the differentiation by  $\eta$  for simplicity.

The one-loop contribution to the effective action induced from the action

Eq. (18) with the effective four-dimensional operator is

$$p_{1,1}^{\text{eff}} = \frac{1}{k} \frac{\partial}{\partial \eta} \left[ \text{tr} \ln [D_q] \right], \quad (\text{C.2})$$

where  $D_q$  is defined in Eq. (30) and the trace is taken on the four-dimensional lattice sites, color, and spinor indices. The effective four-dimensional operator is renormalized by  $Z$  and  $am_{\text{res}}$  according to Eqs. (30), (21), and (22). We show  $p_{1,1} = p_{1,1}^{\text{eff}}$  in the following.

Substituting Eqs. (10) and (30) into Eq. (C.2), we have

$$p_{1,1}^{\text{eff}} = \frac{1}{k} \text{tr} \left[ \epsilon^T P^T (D_{\text{MDWF}})^{-1} D_{\text{PV}} P \epsilon \right. \\ \left. \times \epsilon^T P^T \left\{ -(D_{\text{PV}})^{-1} \frac{\partial D_{\text{PV}}}{\partial \eta} D_{\text{PV}}^{-1} D_{\text{MDWF}} + (D_{\text{PV}})^{-1} \frac{\partial D_{\text{MDWF}}}{\partial \eta} \right\} P \epsilon \right]. \quad (\text{C.3})$$

We introduce two matrices  $A$  and  $B$  defined by

$$A = P^T (D_{\text{MDWF}})^{-1} D_{\text{PV}} P, \quad (\text{C.4})$$

$$B = P^T \left\{ (D_{\text{PV}})^{-1} \frac{\partial D_{\text{MDWF}}}{\partial \eta} - (D_{\text{PV}})^{-1} \frac{\partial D_{\text{PV}}}{\partial \eta} (D_{\text{PV}})^{-1} D_{\text{MDWF}} \right\} P. \quad (\text{C.5})$$

to simplify  $p_{1,1}$  and  $p_{1,1}^{\text{eff}}$  as

$$p_{1,1} = \frac{1}{k} \text{Tr} [AB], \quad (\text{C.6})$$

$$p_{1,1}^{\text{eff}} = \frac{1}{k} \text{tr} [(\epsilon^T A \epsilon) (\epsilon^T B \epsilon)], \quad (\text{C.7})$$

where  $PP^T = 1$  is used.

After some matrix algebra in the five-dimensional notation, we obtain

$$A = \left( \begin{array}{c|c} \frac{1 - (1 - m_f)\alpha}{\vec{z}} & 0 \\ \hline & \mathbf{I} \end{array} \right), \quad (\text{C.8})$$

$$B = \left( \begin{array}{c|c} \gamma & 0 \\ \hline \vec{g} & \mathbf{0} \end{array} \right), \quad (\text{C.9})$$

where  $\alpha$  and  $\gamma$  are four-dimensional operators and  $\vec{z}$  and  $\vec{g}$  contain  $N_5 - 1$  four-dimensional operators. Their explicit forms are not required in the proof.

38 *Yuko Murakami and Ken-Ichi Ishikawa*

Substituting Eqs. (C.8) and (C.9) into Eq. (C.6), we obtain

$$\begin{aligned}
 p_{1,1} &= \frac{1}{k} \text{Tr} \left[ \left( \begin{array}{c|c} \frac{1 - (1 - m_f)\alpha}{\vec{z}} & 0 \\ \hline & \mathbf{I} \end{array} \right) \left( \begin{array}{c|c} \gamma & 0 \\ \hline \vec{g} & \mathbf{0} \end{array} \right) \right] \\
 &= \frac{1}{k} \text{tr}[\{1 - (1 - m_f)\alpha\}\gamma], \tag{C.10}
 \end{aligned}$$

where the trace in the last line is now taken only on the four-dimensional lattice, color, and spinor indices.

Similarly substituting Eqs. (C.8) and (C.9) into Eq. (C.7), we obtain

$$\begin{aligned}
 p_{1,1}^{\text{eff}} &= \frac{1}{k} \text{Tr} \left[ (1 \ 0 \ \cdots \ 0) \left( \begin{array}{c|c} \frac{1 - (1 - m_f)\alpha}{\vec{z}} & 0 \\ \hline & \mathbf{I} \end{array} \right) \begin{pmatrix} 1 \\ 0 \\ \vdots \\ 0 \end{pmatrix} \right. \\
 &\quad \left. \times (1 \ 0 \ \cdots \ 0) \left( \begin{array}{c|c} \gamma & 0 \\ \hline \vec{g} & \mathbf{0} \end{array} \right) \begin{pmatrix} 1 \\ 0 \\ \vdots \\ 0 \end{pmatrix} \right] \\
 &= \frac{1}{k} \text{tr}[\{1 - (1 - m_f)\alpha\}\gamma]. \tag{C.11}
 \end{aligned}$$

Thus, we have proved  $p_{1,1} = p_{1,1}^{\text{eff}}$ .

We also note that

$$(D_q)^{-1} = \epsilon^T P^T (D_{\text{MDWF}})^{-1} D_{\text{PV}} P \epsilon, \tag{C.12}$$

holds even with the SF boundary term.

## References

1. P. Hasenfratz, Nucl. Phys. B **525**, 401 (1998) [hep-lat/9802007].
2. P. Hasenfratz, V. Laliena and F. Niedermayer, Phys. Lett. B **427**, 125 (1998) [hep-lat/9801021].
3. D. B. Kaplan, Phys. Lett. B **288**, 342 (1992) [hep-lat/9206013].
4. R. Narayanan and H. Neuberger, Phys. Lett. B **302**, 62 (1993) [hep-lat/9212019].
5. R. Narayanan and H. Neuberger, Phys. Rev. Lett. **71**, 3251 (1993) [hep-lat/9308011].
6. R. Narayanan and H. Neuberger, Nucl. Phys. B **412**, 574 (1994) [hep-lat/9307006].
7. P. H. Ginsparg and K. G. Wilson, Phys. Rev. D **25**, 2649 (1982).
8. M. Lüscher, Phys. Lett. B **428**, 342 (1998) [hep-lat/9802011].
9. M. Creutz, Rev. Mod. Phys. **73**, 119 (2001) [hep-lat/0007032].
10. H. Neuberger, Ann. Rev. Nucl. Part. Sci. **51**, 23 (2001) [hep-lat/0101006].
11. S. Chandrasekharan and U. J. Wiese, Prog. Part. Nucl. Phys. **53**, 373 (2004) [hep-lat/0405024].

12. S. Aoki *et al.*, *Eur. Phys. J. C* **74**, 2890 (2014), arXiv:1310.8555 [hep-lat].
13. G. Martinelli, S. Petrarca, C. T. Sachrajda and A. Vladikas, *Phys. Lett. B* **311**, 241 (1993) [Erratum-ibid. *B* **317**, 660 (1993)].
14. G. Martinelli, C. Pittori, C. T. Sachrajda, M. Testa and A. Vladikas, *Nucl. Phys. B* **445**, 81 (1995) [hep-lat/9411010].
15. M. Lüscher, R. Narayanan, P. Weisz and U. Wolff, *Nucl. Phys. B* **384**, 168 (1992) [hep-lat/9207009].
16. S. Sint, *Nucl. Phys. B* **421**, 135 (1994) [hep-lat/9312079].
17. M. Lüscher, R. Sommer, P. Weisz and U. Wolff, *Nucl. Phys. B* **413**, 481 (1994) [hep-lat/9309005].
18. S. Sint, *Nucl. Phys. B* **451**, 416 (1995) [hep-lat/9504005].
19. M. Lüscher, *JHEP* **1008**, 071 (2010) [Erratum-ibid. **1403**, 092 (2014)] [arXiv:1006.4518 [hep-lat]].
20. M. Lüscher and P. Weisz, *JHEP* **1102**, 051 (2011) [arXiv:1101.0963 [hep-th]].
21. Z. Fodor, K. Holland, J. Kuti, D. Nogradi and C. H. Wong, *JHEP* **1211**, 007 (2012) [arXiv:1208.1051 [hep-lat]].
22. P. Fritzsche and A. Ramos, *JHEP* **1310**, 008 (2013) [arXiv:1301.4388 [hep-lat]].
23. H. Suzuki, *PTEP* **2013**, no. 8, 083B03 (2013) [arXiv:1304.0533 [hep-lat]].
24. M. Lüscher, *JHEP* **1304**, 123 (2013) [arXiv:1302.5246 [hep-lat]].
25. M. Lüscher and P. Weisz, *Nucl. Phys. B* **479**, 429 (1996) [hep-lat/9606016].
26. M. Lüscher, S. Sint, R. Sommer, P. Weisz and U. Wolff, *Nucl. Phys. B* **491**, 323 (1997) [hep-lat/9609035].
27. M. Lüscher, S. Sint, R. Sommer and H. Wittig, *Nucl. Phys. B* **491**, 344 (1997) [hep-lat/9611015].
28. K. Jansen *et al.* [ALPHA Collaboration], *Nucl. Phys. B* **530**, 185 (1998) [Erratum-ibid. *B* **643**, 517 (2002)] [hep-lat/9803017].
29. S. Capitani *et al.* [ALPHA Collaboration], *Nucl. Phys. B* **544**, 669 (1999) [hep-lat/9810063].
30. S. Sint *et al.* [ALPHA Collaboration], *Nucl. Phys. B* **545**, 529 (1999) [hep-lat/9808013].
31. A. Bode *et al.* [ALPHA Collaboration], *Phys. Lett. B* **515**, 49 (2001) [hep-lat/0105003].
32. M. Della Morte *et al.* [ALPHA Collaboration], *Nucl. Phys. B* **713**, 378 (2005) [hep-lat/0411025].
33. M. Guagnelli *et al.* [ALPHA Collaboration], *JHEP* **0603**, 088 (2006) [hep-lat/0505002].
34. M. Della Morte *et al.* [ALPHA Collaboration], *Nucl. Phys. B* **729**, 117 (2005) [hep-lat/0507035].
35. P. Dimopoulos *et al.* [ALPHA Collaboration], *JHEP* **0805**, 065 (2008) [arXiv:0712.2429 [hep-lat]].
36. Y. Taniguchi, *JHEP* **0610**, 027 (2006) [hep-lat/0604002].
37. Y. Taniguchi, *JHEP* **0512**, 037 (2005) [hep-lat/0412024].
38. M. Lüscher, *JHEP* **0605**, 042 (2006) [hep-lat/0603029].
39. S. Takeda, *Nucl. Phys. B* **796**, 402 (2008) [arXiv:0712.1469 [hep-lat]].
40. S. Takeda, *Phys. Rev. D* **87**, no. 11, 114506 (2013) [arXiv:1010.3504 [hep-lat]].
41. S. Sint, *PoS LAT* **2007**, 253 (2007).
42. R. C. Brower, H. Neff and K. Orginos, *Nucl. Phys. Proc. Suppl.* **140**, 686 (2005) [hep-lat/0409118].
43. R. C. Brower, H. Neff and K. Orginos, arXiv:1206.5214 [hep-lat].
44. S. Hashimoto, S. Aoki, G. Cossu, H. Fukaya, T. Kaneko, J. Noaki and P. A. Boyle, *PoS LATTICE* **2013**, 431 (2014).
45. Y. Murakami and K. I. Ishikawa, *PoS LATTICE* **2014**, 331 (2014) [arXiv:1410.8335].

40 *Yuko Murakami and Ken-Ichi Ishikawa*

- [hep-lat]].
46. Y. Murakami and K. I. Ishikawa, PoS LATTICE **2015**, 308 (2016) [arXiv:1701.07139 [hep-lat]].
  47. Y. Kikukawa and T. Noguchi, hep-lat/9902022.
  48. Y. Kikukawa, Nucl. Phys. B **584**, 511 (2000) [hep-lat/9912056].
  49. S. Capitani, PoS LAT **2007**, 066 (2007) [arXiv:0708.3281 [hep-lat]].
  50. A. Boriçi, Nucl. Phys. Proc. Suppl. **83** (2000) 771 [hep-lat/9909057].
  51. A. Boriçi, in Lattice Fermions and Structure of the Vacuum, V. Mitrjushkin *et al.* (eds.), Springer 2000, [hep-lat/9912040].
  52. A. Boriçi, in QCD and numerical analysis III, A. Boriçi *et al.* (eds.), Springer 2005, [hep-lat/0402035].
  53. T. W. Chiu, Phys. Rev. Lett. **90**, 071601 (2003) [hep-lat/0209153].
  54. V. Furman and Y. Shamir, Nucl. Phys. B **439**, 54 (1995) [hep-lat/9405004].
  55. Y. C. Chen and T. W. Chiu, Phys. Lett. B **738**, 55 (2014) [arXiv:1403.1683 [hep-lat]].
  56. K. Ogawa *et al.* [TWQCD Collaboration], PoS LAT **2009**, 033 (2009) [arXiv:0911.5532 [hep-lat]].
  57. P. A. Boyle [UKQCD Collaboration], PoS LATTICE **2014** (2015) 087.
  58. T. W. Chiu, Phys. Lett. B **744** (2015) 95 [arXiv:1503.01750 [hep-lat]].
  59. T. W. Chiu, T. H. Hsieh, C. H. Huang and T. R. Huang, Phys. Rev. D **66**, 114502 (2002) [hep-lat/0206007].
  60. H. J. Rothe, *World Sci. Lect. Notes Phys.* **43**, 1 (1992) [*World Sci. Lect. Notes Phys.* **59**, 1 (1997); *ibid.* **74**, 1 (2005); **82**, 1 (2012)].
  61. C. Itzykson and J. B. Zuber, “Quantum Field Theory,” McGraw-Hill Book Co., New York, 1988.
  62. S. Sint and R. Sommer, Nucl. Phys. B **465** (1996) 71 [hep-lat/9508012].
  63. S. Sint, Nucl. Phys. B **847** (2011) 491 [arXiv:1008.4857 [hep-lat]].
  64. M. Luscher, S. Sint, R. Sommer and P. Weisz, Nucl. Phys. B **478** (1996) 365 [hep-lat/9605038].
  65. S. Aoki and Y. Kuramashi, Phys. Rev. D **68** (2003) 034507 [hep-lat/0306008].
  66. C. Alexandrou, H. Panagopoulos and E. Vicari, Nucl. Phys. B **571** (2000) 257 [hep-lat/9909158].
  67. M. Lüscher, P. Weisz and U. Wolff, Nucl. Phys. B **359**, 221 (1991).